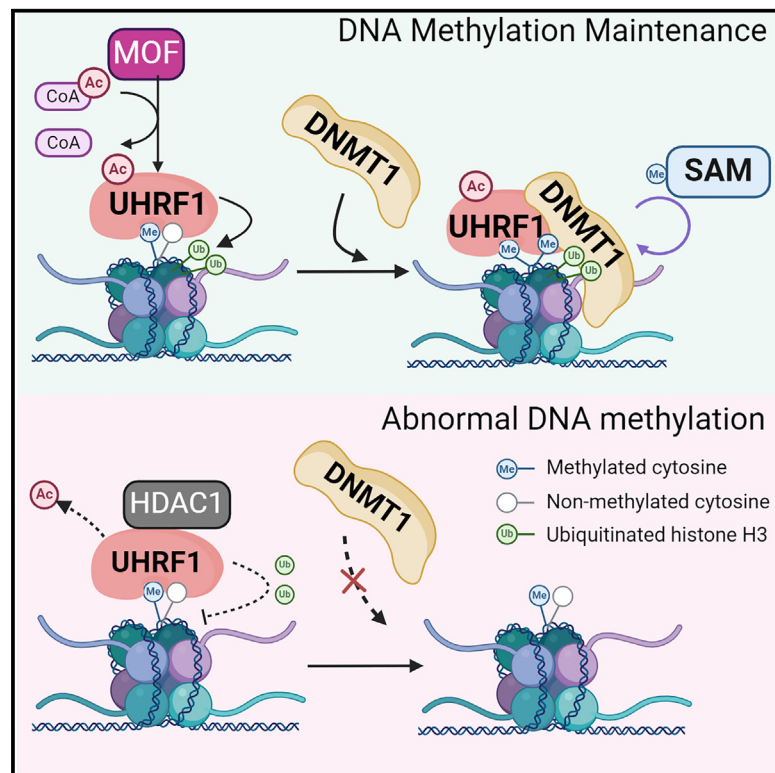# MOF-mediated acetylation of UHRF1 enhances UHRF1 E3 ligase activity to facilitate DNA methylation maintenance

Graphical abstract

Authors

Linsheng Wang, Xi Yang, Kaiqiang Zhao, ..., Xiaobin Hu, Guoxiang Jin, Zhongjun Zhou

Correspondence

jinguoxiang@gdph.org.cn (G.J.), zhongjun@hku.hk (Z.Z.)

In brief

Wang et al. describe a regulatory mechanism of UHRF1 in DNA methylation maintenance. UHRF1 acetylation by MOF at lysine 670 is essential for efficient DNMT1 recruitment by facilitating histone H3 ubiquitination. These findings suggest that UHRF1 acetylation is important for its E3 ubiquitin ligase function in various biological processes.

Highlights

- MOF acetylates UHRF1 at K670, which is counteracted by HDAC1

- Acetylation by MOF enhances UHRF1 E3 ubiquitin ligase activity

- Abolishment of UHRF1 acetylation impairs histone H3 ubiquitination and DNMT1 recruitment

- K670 acetylation of UHRF1 is required for proper function of DNA methylation maintenance

CellPress

Article

MOF-mediated acetylation of UHRF1 enhances UHRF1 E3 ligase activity to facilitate DNA methylation maintenance

Linsheng Wang,[1,2,3,6] Xi Yang,[3,6] Kaiqiang Zhao,[3,4] Shengshuo Huang,[3] Yiming Qin,[1,2] Zixin Chen,[1,2] Xiaobin Hu,[3] Guoxiang Jin,[2,*] and Zhongjun Zhou[2,3,5,7,*]

[1]Guangdong Cardiovascular Institute, Guangdong Provincial People's Hospital, Guangdong Academy of Medical Sciences, Guangzhou, P.R. China
[2]Medical Research Institute, Guangdong Provincial People's Hospital (Guangdong Academy of Medical Sciences), Southern Medical University, Guangzhou, P.R. China
[3]School of Biomedical Sciences, The University of Hong Kong, Pok Fu Lam, Hong Kong
[4]Dongguang Children's Hospital, Dongguan Pediatric Research Institute, Dongguan, P.R. China
[5]Orthopedic Center, The University of Hong Kong-Shenzhen Hospital, Shenzhen, P.R. China
[6]These authors contributed equally
[7]Lead contact
*Correspondence: jinguoxiang@gdph.org.cn (G.J.), zhongjun@hku.hk (Z.Z.)
https://doi.org/10.1016/j.celrep.2024.113908

SUMMARY

The multi-domain protein UHRF1 (ubiquitin-like, containing PHD and RING finger domains, 1) recruits DNMT1 for DNA methylation maintenance during DNA replication. Here, we show that MOF (males absent on the first) acetylates UHRF1 at K670 in the pre-RING linker region, whereas HDAC1 deacetylates UHRF1 at the same site. We also identify that K667 and K668 can also be acetylated by MOF when K670 is mutated. The MOF/HDAC1-mediated acetylation in UHRF1 is cell-cycle regulated and peaks at G1/S phase, in line with the function of UHRF1 in recruiting DNMT1 to maintain DNA methylation. In addition, UHRF1 acetylation significantly enhances its E3 ligase activity. Abolishing UHRF1 acetylation at these sites attenuates UHRF1-mediated H3 ubiquitination, which in turn impairs DNMT1 recruitment and DNA methylation. Taken together, these findings identify MOF as an acetyltransferase for UHRF1 and define a mechanism underlying the regulation of DNA methylation maintenance through MOF-mediated UHRF1 acetylation.

INTRODUCTION

UHRF1 (ubiquitin-like, containing plant homeodomain [PHD] and RING finger domains, 1), a multi-domain protein, functions as an epigenetic modifier.[1] UHRF1 is known for its essential role in maintaining DNA CpG methylation during DNA replication.[2,3] The distinct functions of five different domains of UHRF1 in the maintenance of DNA methylation have been extensively investigated in the past few years. During DNA replication, proliferating cell nuclear antigen (PCNA), together with methylated DNA ligase 1, recruits UHRF1 to the replication foci, where the SET and RING-associated (SRA) domain of UHRF1 recognizes and binds to the hemi-methylated DNA.[2–5] The Tudor/PHD domain of UHRF1 binds to unmodified H3R2 and methylated H3K9 to facilitate UHRF1's localization to the nascent DNA.[6–8] The C-terminal RING finger domain confers UHRF1 with E3 ubiquitin ligase activity. Upon recognizing hemi-methylated DNA and binding to the histone near the nascent DNA, UHRF1 can mono-ubiquitinate histone H3 at K18 and K23, the modifications that are essential for DNMT1 recruitment.[9,10] We and others also revealed that the dually ubiquitinated histone H3 (H3K18ub and

H3K23ub, respectively) interacts with the replication focus targeting sequence (RFTS) domain of DNMT1, which is not only responsible for the localization of DNMT1 to the newly synthesized DNA but also results in DNMT1 activation due to the spatial rearrangement of C-lobes in the RFTS domain.[9,11,12] Taken together, efficient DNMT1 recruitment mediated by UHRF1 following DNA replication establishes the proper maintenance of DNA methylation.

Similar to the ubiquitination of histone H3, UHRF1 also targets other substrates for non-degradative ubiquitination, including PAF15 (PCNA-associated factor 15), Tip60 (KAT5, lysine acetyltransferase 5), and p53.[13–16] Moreover, UHRF1 could perform poly-ubiquitination on DNMT1 to promote its removal and degradation when cells exit the replication S phase.[17,18] It also ubiquitinates and degrades DNMT3A (DNA methyltransferase 3 alpha) and tumor-suppressor promyelocytic leukemia (PML) gene to promote tumorigenesis.[19,20]

Post-translational modifications are important in regulating protein functions. The phosphorylation of UHRF1 at different serine sites promotes various biological functions such as transcriptional activation of gene expression, histone binding,

protein stability, and DNA damage response.[21–24] UHRF1 is ubiquitinated by β-transducin-repeat-containing protein (TrCP) and also by itself.[24,25] Methylation of UHRF1 at K385 by SET7 (SET domain containing 7) facilitates the homologous-recombination-mediated DNA damage repair.[26] Interestingly, UHRF1 co-exists with DNMT1, acetyltransferase Tip60, and deacetylase HDAC1 (histone deacetylase 1) in the same complex.[13,17,27] Acetylation of DNMT1 by Tip60 destabilizes DNMT1 at the end of the S phase to facilitate its removal and ubiquitination-dependent degradation by UHRF1, while HDAC1 in this complex could de-acetylate and stabilize DNMT1 during early and middle S phase. However, little is known about the acetylation of UHRF1 in the complex and its impact on DNA methylation maintenance. A recent study showed that maintaining the de-acetylated state of UHRF1 at K490 enhances its binding affinity to hemi-methylated DNA,[28] highlighting the potential role of UHRF1 acetylation in DNA methylation maintenance during replication.

In this study, we identified MOF (males absent on the first), an MYST family acetyltransferase, as a predominant acetyltransferase for UHRF1, while HDAC1 facilitated the de-acetylation of UHRF1 at the same sites. K670 in the pre-RING linker regions of UHRF1 was found to be acetylated by MOF resolved by mass spectrometry and site-directed mutagenesis, while K667 and K668 could also be acetylated by MOF when K670 was mutated. We further revealed that MOF/HDAC1-mediated UHRF1 acetylation enhanced the E3 ligase activity of UHRF1 toward histone H3. Our data suggested that the modulation of H3 ubiquitination through the dynamic acetylation of UHRF1 during the cell cycle is critical for efficient DNMT1 recruitment and DNA methylation maintenance.

RESULTS

MOF and HDAC1 are acetyltransferase and de-acetylase for UHRF1, respectively

The phosphorylation and ubiquitination modifications of UHRF1 have been shown to have biological relevance.[21–25] Recently, UHRF1 was also identified as an acetylated protein mediated by PCAF and HDAC1.[28] To further investigate whether other acetyltransferases could also acetylate UHRF1, a cell-based acetylation assay was performed in HEK293T cells with ectopic UHRF1 and different histone acetyltransferases (HATs), including MYST family HATs MOF, Tip60, and HBO1, p300/CBP family acetyltransferase p300, and GNAT family GCN5. As shown in Figure 1A, among the five HATs tested, only MOF significantly increased UHRF1 acetylation.

MOF is a known acetyltransferase belonging to the MYST family[29] and acetylates histone H4 at K16/K12/K8.[30] It also targets non-histone substrates such as p53 at K120.[31] To verify that MOF acetylated UHRF1, we then performed a cell-based acetylation assay in HEK293T cells expressing ectopic UHRF1 together with either the full-length MOF or catalytic-domain-deleted MOF (1–130 aa). Ectopic expression of the full-length MOF resulted in a dramatic increase in UHRF1 acetylation, while the truncated MOF lacking a catalytic domain failed to increase UHRF1 acetylation compared to the controls (Figure S1A). Immunoprecipitation in 293T cells exhibited significantly increased acetylation in the endogenous UHRF1 in the presence of ectopic

MOF (Figure 1B). Moreover, the acetylation assay employing purified glutathione S-transferase (GST)-tagged UHRF1 and MOF demonstrated that MOF could directly acetylate UHRF1 (Figure 1C). To further substantiate the observation that MOF acetylates UHRF1, we knocked down MOF by small interfering RNA to examine the UHRF1 acetylation. FLAG-Myc-tagged UHRF1 exhibited a significantly decreased acetylation upon MOF knockdown (Figure 1D). The immunoprecipitation showed the interaction between endogenous MOF and UHRF1, which was confirmed by the reciprocal co-immunoprecipitation of ectopic FLAG-Myc-UHRF1 and EGFP-MOF (Figures S1B–S1E). Collectively, these data suggest that UHRF1 is a substrate for MOF-mediated acetylation.

As UHRF1 is the component of a protein complex with HDAC1, which de-acetylates UHRF1 at K490,[13,17,27,28] we then asked whether HDAC1 serves as a deacetylase at sites of MOF-mediated UHRF1 acetylation. In agreement with the previous observation, the acetylation of UHRF1 significantly decreased upon ectopic HDAC1 expression (Figure 1E). Interestingly, MOF-mediated increase in UHRF1 acetylation was attenuated by ectopic HDAC1 in 293T cells (Figure S1F), suggesting that MOF-mediated UHRF1 acetylation can be removed by HDAC1. The attenuation of UHRF1 acetylation by HDAC1 was restored in the presence of 1 mM sodium butyrate (NaB) (Figure S1G), a known class I HDAC inhibitor, specifically for HDAC1, HDAC2, and HDAC3.[32] Higher levels of NaB treatment (2 or 5 mM) could also increase the acetylation levels of ectopic UHRF1 without ectopic HDAC1 (Figure S1H), while 5 mM NaB or HDACI/II inhibitor trichostatin A (TSA) treatment could efficiently increase the acetylation levels on endogenous UHRF1 (Figure S1I). In agreement with previous work showing that UHRF1 and HDAC1 are in the same protein complex,[27,28] reciprocal co-immunoprecipitation in HEK293T cells revealed the interaction between endogenous UHRF1 and HDAC1 (Figure S1J).

Taken together, these data indicated that UHRF1 is predominantly acetylated by MOF and de-acetylated by HDAC1. Interestingly, MOF-mediated UHRF1 acetylation can be removed by HDAC1, suggesting that UHRF1 acetylation is likely modulated through the balance between MOF and HDAC1 activities.

MOF acetylates UHRF1 around K670 in the pre-RING linker region

To identify the functional domains in UHRF1 that MOF acetylates, we co-expressed the full-length, or domain-deleted, UHRF1 constructs together with FLAG-tagged MOF in HEK293T cells. Cell lysates were subjected to immunoprecipitation using FLAG antibodies, and then we analyzed the pan-acetyl-lysine antibodies. Surprisingly, while individual domain deletion (RING, SRA, PHD, and UBL) in UHRF1 did not result in the significant attenuation in MOF-mediated acetylation, removing SRA, the pre-RING linker region, and the RING domain together completely abolished MOF-mediated acetylation (Figure 2A). The in vitro acetylation assay using various domain-deleted UHRF1 proteins revealed that the major acetylation sites in UHRF1 meditated by MOF resided in the pre-RING linker regions (Figure S2A). These experiments indicated that MOF likely targets the pre-RING linker region for acetylation. To further confirm this observation, we generated mutant UHRF1 plasmids with pre-RING linker region deletion. As
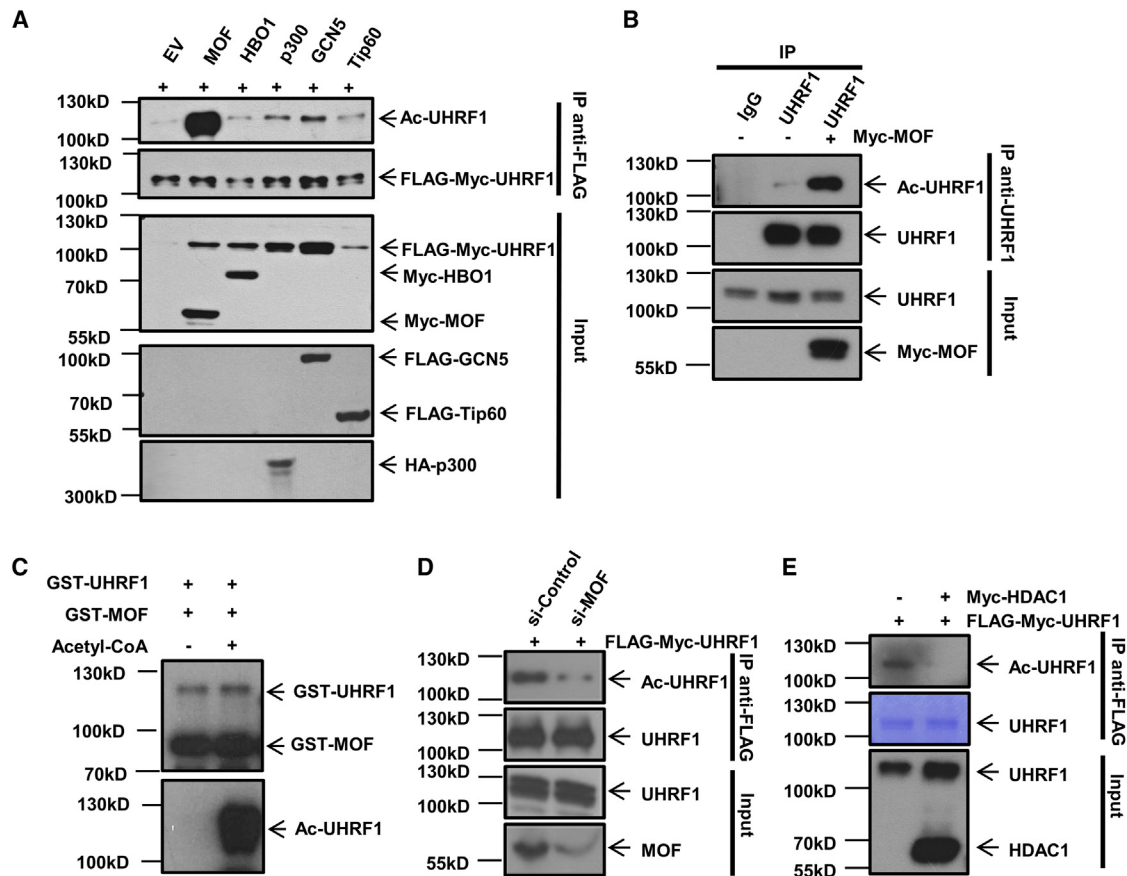
Figure 1. UHRF1 is acetylated specifically by MOF and de-acetylated by HDAC1

(A) FLAG-Myc-UHRF1 and different HATs were co-expressed in HEK293T cells. The cell lysates were immunoprecipitated with FLAG antibody and subjected to immunoblotting with acetyl-lysine antibodies to detect acetylated UHRF1. EV represents empty vector control.

(B) Empty vector or Myc-MOF plasmids were transfected into HEK293T cells. Endogenous UHRF1 was immunoprecipitated 48 h after transfection and subjected to western blotting with UHRF1 and pan-acetyl-lysine antibodies. Immunoglobulin G (IgG) was used as a control of the UHRF1 antibodies in the immunoprecipitation (IP).

(C) In vitro acetylation assays were done by incubating purified GST-UHRF1 and GST-MOF with acetyl-CoA. Control assays were performed without acetyl-CoA. Acetylation of UHRF1 was detected by acetyl-lysine antibodies. UHRF1 and MOF proteins were examined using GST antibodies.

(D) Control and MOF small interfering RNA (siRNA) were transfected into HEK293T cells with ectopic FLAG-Myc-UHRF1. The cell lysates were immunoprecipitated with FLAG antibody and subjected to western blotting with antibodies against FLAG and acetyl-lysine.

(E) IP with FLAG antibody in HEK293T cells transfected with FLAG-Myc-UHRF1 together with either empty vector or Myc-HDAC1, followed by western blotting with antibodies against pan-acetyl-lysine, UHRF1, and HDAC1. Coomassie blue staining was done to confirm equal loading of UHRF1 in IP samples.

expected, deletion of the pre-RING linker region (587–723 aa) completely abolished MOF-mediated acetylation in UHRF1 (Figure 2B). Further deletion analysis revealed that the C terminus of UHRF1 between amino acids 601 and 793 is critical for MOF-mediated acetylation (Figure S2B).

Previous reports predicted the potential acetylation sites of UHRF1 at K399, K490, and K546.[28,33] To further identify the specific lysine residues in full-length UHRF1 modified by MOF, mass spectrometry was employed to analyze the MOF-mediated acetylation sites. Upon *in vitro* incubation with UHRF1 protein with MOF and acetyl-coenzyme A (CoA), several lysine residuals were found to have increased acetylation (Figures 3A and S3). Based on the previous observation that acetylation required the fragment of 601–723 aa, we then paid particular attention to the K670 residue within this region, which had the highest in-

tensity score in the mass spectrometry analysis. We performed site-directed mutagenesis to test whether MOF acetylates UHRF1 at these sites by a cell-based acetylation assay. As shown in Figures 3B and S2C, a K670R mutation (lysine mutated to arginine) in the C-terminal UHRF1 fragment (601–793 aa) could significantly reduce MOF-mediated acetylation, while the other identified lysine site K644R/K646R double mutations or K644R/K646R/K648R/K650R mutations in the 601–723 aa region could not. However, a K670R mutation in the full-length UHRF1 did not show attenuation of MOF-mediated UHRF1 acetylation (Figure 3C). The amino acids from 643 to 657 have been reported to form a polybasic region, within which K644, K646, K648, and K650 together mediate UHRF1's association with heterochromatin.[34] By checking the sequence of UHRF1, we found another lysine cluster in amino acid 601–723 regions, including
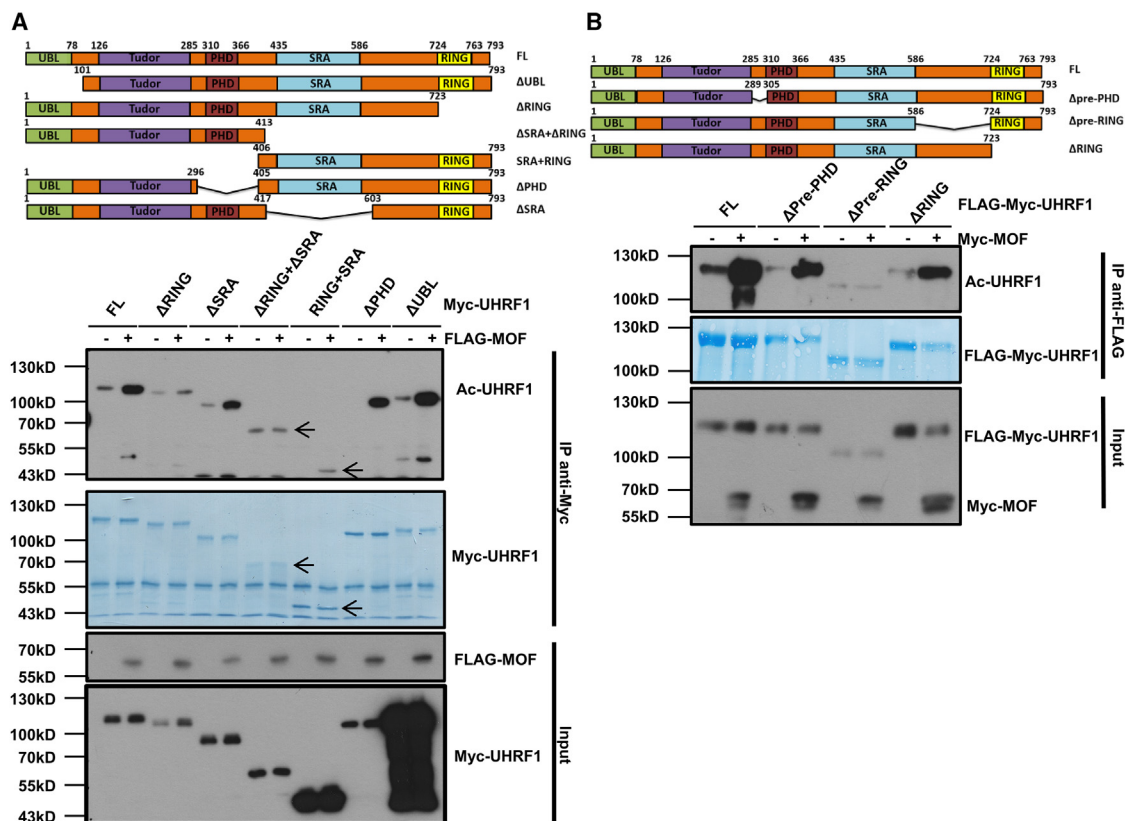
Figure 2. MOF acetylates UHRF1 in the pre-RING linker region

(A) Schematic diagram illustrating the wild-type UHRF1 and domain-deleted UHRF1 mutants used in acetylation analyses (top). HEK293T cells were transiently transfected with different Myc-tagged UHRF1 constructs alone or with FLAG-MOF. Eluates from input and Myc IP were analyzed by western blotting with antibodies against Myc, FLAG, or acetyl-lysine (bottom). Coomassie blue staining was done to show the total UHRF1 protein level in IP samples. ΔRING+ΔSRA and RING+SRA bands in the IP samples were indicated with arrows.

(B) Schematic diagram illustrating the UHRF1 and inter-domain region deleted constructs used in acetylation analyses (top). The inter-domain region deleted UHRF1 mutant constructs were generated by site-directed mutagenesis. HEK293T cells were transiently transfected with UHRF1 constructs alone or with Myc-MOF. Inputs and eluates from FLAG-IP were analyzed by western blotting analysis with antibodies against Myc and pan-acetyl-lysine. Coomassie blue staining was done to show the loading of UHRF1 in the IP samples.

K667, K668, and K670. Interestingly, while both K670R and K667R/K668R mutations reduced the MOF-mediated acetylation in C-terminal-truncated UHRF1 (601–723 aa), only the triple lysine to arginine mutations (K667R/K668R/K670R [3KR]) significantly attenuated the increased acetylation in full-length and C-terminal-truncated UHRF1 mediated by MOF (Figures 3C and S2C). The *in vitro* acetylation assay using purified GST-tagged wild-type or 3KR mutant UHRF1 together with purified GST-MOF, in the presence or absence of acetyl-CoA, confirmed that 3KR mutations led to a significant loss of acetylation in UHRF1 compared to wild-type UHRF1 (Figure 3D). To exclude the possibility that 3KR mutations affect the interaction between UHRF1 and MOF and indirectly attenuate MOF-mediated UHRF1 acetylation, we further performed a cell-based assay and a test tube binding assay to determine MOF binding affinity with wild-type and 3KR mutant UHRF1. Though the pre-RING linker region seemed critical for the efficient binding between UHRF1 and MOF, the 3KR mutation did not impair their interaction (Figures S2D–S2F).

Therefore, by domain mapping, we narrowed down the MOF-mediated acetylated region in UHRF1 to amino acids 601–723. By mass spectrometry, site-directed mutagenesis, and cell-based and *in vitro* acetylation assay, we identified K670 as the predominant site for MOF/HDAC1-mediated UHRF1 acetylation/de-acetylation, while K667 and K668 could also be acetylated by MOF *in vivo* when K670 is mutated.

MOF acetylates UHRF1 during the G1 and S phases and facilitates DNA methylation

Previous reports showed that the protein level of UHRF1, which peaks at the G1 and S phases and is down-regulated at the G2/M phase, is tightly cell-cycle regulated.[35,36] UHRF1 S652 phosphorylation, which peaks at the G2/M phase to ensure UHRF1 removal and degradation, was also identified to be cell-cycle dependent.[36] Given the critical role of UHRF1 in the maintenance of DNA methylation, we postulated that MOF-mediated UHRF1 acetylation could also be regulated in a cell-cycle-dependent manner. To test this hypothesis, UHRF1
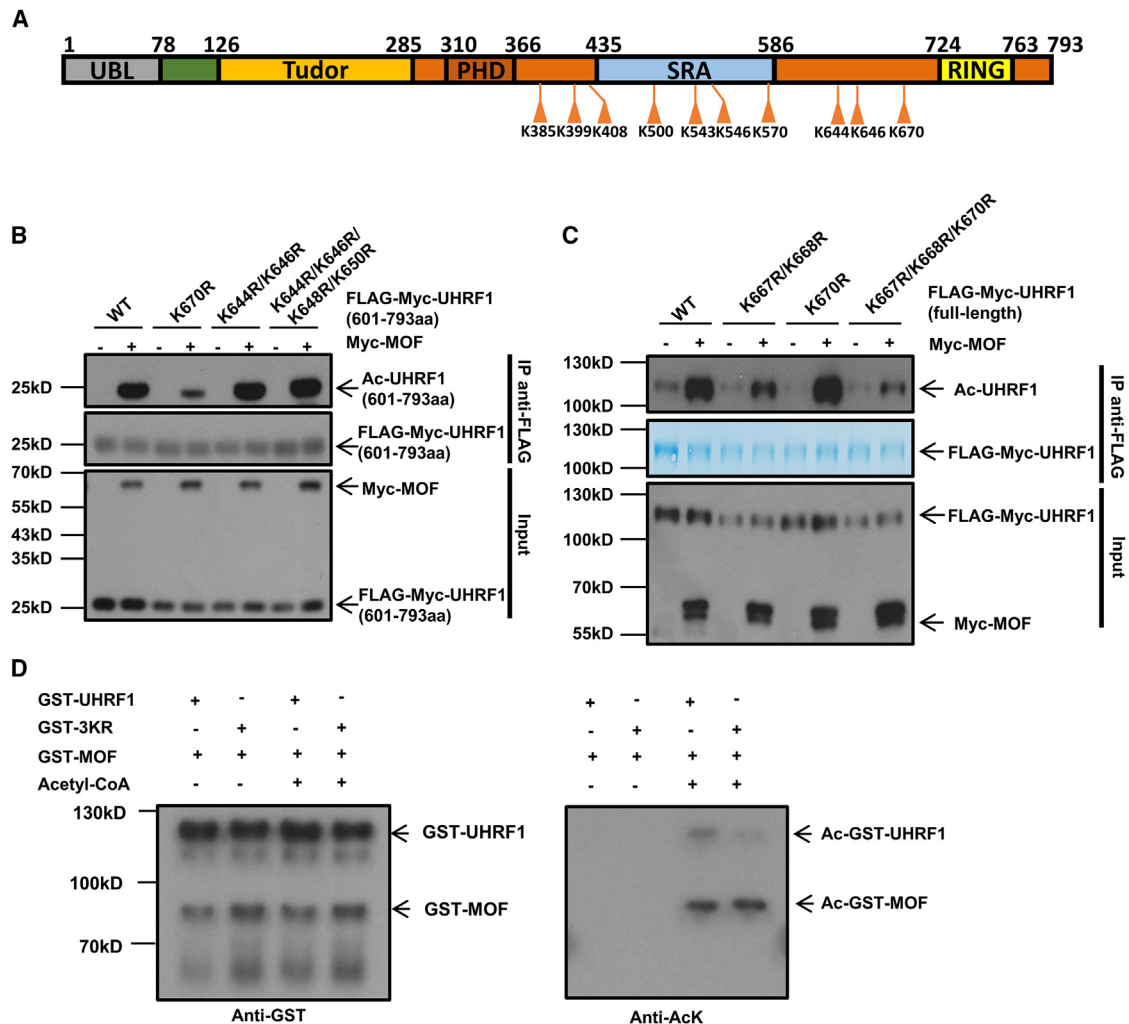
Figure 3. Identification of MOF-mediated acetylation sites in UHRF1 by site-directed mutagenesis

(A) Schematic representation of top 10 scored acetylated lysines in UHRF1 identified by mass spectrometry.

(B) Acetylation of wild-type UHRF1 fragment (601–793 aa) and various mutant UHRF1 fragments (601–793 aa) in the presence or absence of MOF. The ectopic wild-type UHRF1 fragment and different mutant UHRF1 fragments were immunoprecipitated by FLAG antibody followed by western blotting analysis by pan-acetyl-lysine antibodies. Inputs were analyzed with Myc antibodies for the expression of exogenous UHRF1 fragments and MOF.
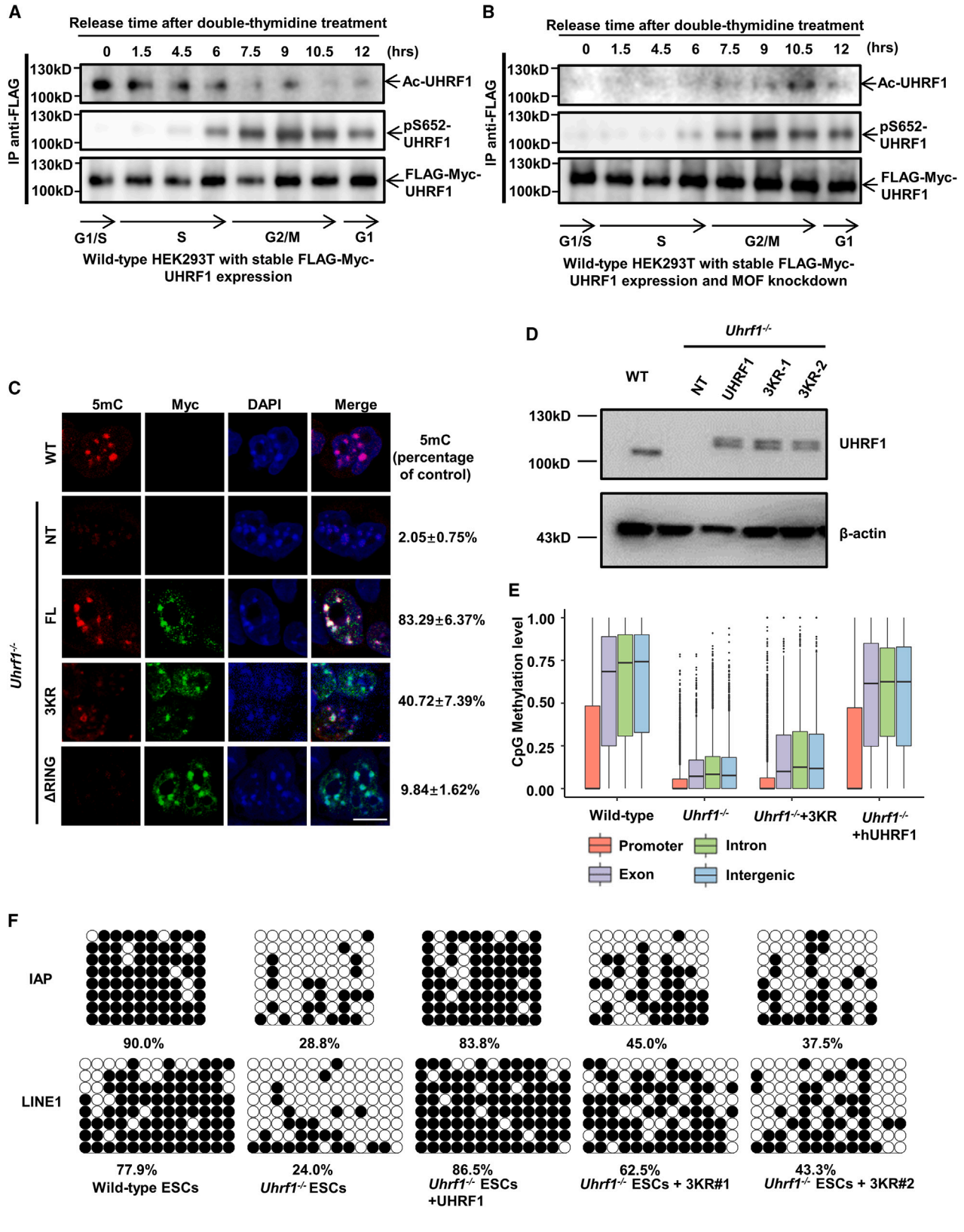
(C) Lysine-to-arginine mutagenesis was generated in the lysine clusters of K667/K668/K670 in FLAG-Myc-UHRF1 plasmids. HEK293T cells were transiently transfected with full-length FLAG-Myc-tagged wild-type or UHRF1 point-mutation constructs alone or with Myc-MOF. Inputs and eluates from FLAG IP were analyzed by western blotting analysis with antibodies against Myc and acetyl-lysine. Coomassie blue staining was done to confirm relative comparable loading of UHRF1 in IP samples.

(D) In vitro acetylation assays were performed by incubating purified GST-UHRF1 or mutant K667R/K668R/K670R (3KR)-UHRF1 and GST-MOF with acetyl-CoA. Control assays were performed without acetyl-CoA. Acetylation of UHRF1 was detected by acetyl-lysine antibodies. UHRF1 and MOF proteins were examined using GST antibodies.

acetylation and S652 phosphorylation were analyzed in synchronized HEK293T cells stably expressing FLAG-Myc-tagged UHRF1. As expected, S652p-UHRF1 peaked at the G2/M phase and was down-regulated at the G1 and S phase (Figures 4A, 4B, and S4), serving as a good marker for cell cycle. As shown in Figures 4A and S4B, the acetylation of wild-type UHRF1 exhibited a complementary pattern, which peaked at the G1/S phase while decreasing at the G2/M phase. Notably, the elevated UHRF1 acetylation at the S phase was attenuated in cells with MOF knockdown or 3KR mutant FLAG-Myc-tagged

UHRF1 expression (Figures 4B and S4C), suggesting that MOF-mediated UHRF1 acetylation is cell-cycle dependent and mainly in the S phase.

Since UHRF1 is essential for DNA methylation maintenance during DNA replication in the S phase, it was plausible that MOF-mediated acetylation of UHRF1 has a biological relevance, which is most likely related to the DNA methylation maintenance. To address this question, we employed wild-type and *Uhrf1*^{−/−} mouse embryonic stem cells (ESCs) to check how changes in acetylation of UHRF1 would affect

A

Release time after double-thymidine treatment

| | 0 | 1.5 | 4.5 | 6 | 7.5 | 9 | 10.5 | 12 | (hrs) |

IP anti-FLAG

← Ac-UHRF1

← pS652-UHRF1

← FLAG-Myc-UHRF1

G1/S → S → G2/M → G1

Wild-type HEK293T with stable FLAG-Myc-UHRF1 expression

B

Release time after double-thymidine treatment

| | 0 | 1.5 | 4.5 | 6 | 7.5 | 9 | 10.5 | 12 | (hrs) |

IP anti-FLAG

← Ac-UHRF1

← pS652-UHRF1

← FLAG-Myc-UHRF1

G1/S → S → G2/M → G1

Wild-type HEK293T with stable FLAG-Myc-UHRF1 expression and MOF knockdown

C

5mC Myc DAPI Merge

5mC (percentage of control)

WT

Uhrf1⁻/⁻

NT — 2.05±0.75%

FL — 83.29±6.37%

3KR — 40.72±7.39%

ΔRING — 9.84±1.62%

D

Uhrf1⁻/⁻

WT | NT | UHRF1 | 3KR-1 | 3KR-2

UHRF1

β-actin

E

CpG Methylation level

Wild-type | *Uhrf1⁻/⁻* | *Uhrf1⁻/⁻*+3KR | *Uhrf1⁻/⁻*+hUHRF1

Promoter Intron
Exon Intergenic

F

IAP

90.0% 28.8% 83.8% 45.0% 37.5%

LINE1

77.9% 24.0% 86.5% 62.5% 43.3%

Wild-type ESCs | *Uhrf1⁻/⁻* ESCs | *Uhrf1⁻/⁻* ESCs +UHRF1 | *Uhrf1⁻/⁻* ESCs + 3KR#1 | *Uhrf1⁻/⁻* ESCs + 3KR#2

(legend on next page)

DNA methylation. The full-length, RING-deleted, or 3KR mutant FLAG-Myc-tagged UHRF1 was stably expressed in $Uhrf1^{-/-}$ mouse ESCs. DNA methylation in these ESCs was examined by immunofluorescent staining with the 5-methylcytosine (5mC) antibodies (Figure 4C). While the wild-type ESCs show high levels of DNA methylation, $Uhrf1^{-/-}$ ESCs exhibited very weak staining of 5mC, indicating that loss of Uhrf1 compromised the maintenance of DNA methylation. Introducing wild-type full-length UHRF1, but not RING-deleted Uhrf1, into $Uhrf1^{-/-}$ ESCs largely restored the global DNA methylation (83.29% vs. 9.84%), consistent with the previous report, as RING-domain-mediated histone H3 ubiquitination is required for proper DNA methylation.[9] Interestingly, introducing 3KR mutant UHRF1 into $Uhrf1^{-/-}$ ESCs did not restore the DNA methylation as efficiently as the wild-type UHRF1 did (40.72% vs. 83.29%) (Figure 4C), suggesting that the acetylation of UHRF1 at K670, K667, or K668 by MOF is required for the proper function of UHRF1 in the process of DNA methylation maintenance. This finding was further substantiated by the bisulfite DNA methylation sequencing analyses of IAP and LINE1 regions in wild-type ESCs, $Uhrf1^{-/-}$ ESCs, and $Uhrf1^{-/-}$ ESCs stably expressing either wild-type or 3KR mutant human UHRF1 (Figures 4D and 4F). As shown in Figure 4F, 3KR mutant UHRF1 could not fully rescue the methyl-cytosine levels in IAP and LINE1 regions in $Uhrf1^{-/-}$ ESCs compared to those in either wild-type ESCs or $Uhrf1^{-/-}$ ESCs expressing human wild-type UHRF1. In addition, reduced representation bisulfite sequencing (RRBS) analyses revealed that ectopic 3KR mutant human UHRF1 failed to rescue the defective CpG methylation in different genomic regions in $Uhrf1^{-/-}$ ESCs, in contrast to the wild-type human UHRF1. (Figure 4E). Gene Ontology (GO) term analysis of the RRBS data revealed that various differentiation-related pathways, such as neurogenesis, Wnt signaling, and muscle cell differentiation, were significantly affected in 3KR mutant cells (Figure S5A).

These observations collectively suggested that MOF-mediated UHRF1 acetylation during G1 and S phases is critical for the maintenance of DNA methylation.

MOF/HDAC1-mediated UHRF1 acetylation is essential for efficient DNMT1 recruitment during DNA methylation maintenance via H3 ubiquitination

To test if the defective DNA methylation maintenance of acetylation mutant UHRF1 is a consequence of the failure in DNMT1 recruitment, we co-immunostained DNMT1 and ectopic FLAG-tagged UHRF1 in ESCs. Consistent with the results in DNA methylation maintenance, while introducing wild-type UHRF1 efficiently recruited DNMT1 to the heterochromatin in $Uhrf1^{-/-}$ ESCs, the recruitment of DNMT1 to the heterochromatin is significantly impaired in $Uhrf1^{-/-}$ ESCs transfected with 3KR mutant UHRF1 (Figure 5A).

It has been reported previously that the K644/K646/K648/K650 lysine cluster mediated the association of UHRF1 with heterochromatin[34] and that the intracellular localization of UHRF1 changed upon the phosphorylation at S661 in UHRF1.[37] Therefore, we asked whether the defective DNMT1 recruitment in $Uhrf1^{-/-}$ ESCs with 3KR mutant UHRF1 expression results from the mis-localization of UHRF1. As shown in Figures S6A–S6C, no obvious change of the hypo-acetylated UHRF1 (3KR mutant) was observed in the nuclear localization or the heterochromatin association in HeLa, HEK293T, and mouse ESCs. On the other hand, neither hyper-acetylated UHRF1 nor hypo-acetylated UHRF1 disrupted the interaction between DNMT1 and UHRF1 (Figure S6D), suggesting that the acetylation and de-acetylation in UHRF1 did not affect the binding between DNMT1 and UHRF1. Previously, the K490 acetylation in UHRF1 was reported to affect UHRF1 binding affinity with hemi-methylated DNA. However, as shown in Figure S6E, 3KR mutations did not reduce the binding affinity between UHRF1 and hemi-methylated DNA.

UHRF1-mediated histone H3 dual mono-ubiquitination is a prerequisite for DNMT1 recruitment to the newly synthesized DNA during DNA replication.[9,11] Given that the pre-RING linker region of UHRF1 is required for its ubiquitination on p53,[14] we speculated that the acetylation in the pre-RING linker region of UHRF1 may also affect its E3 ligase activity, therefore compromising the H3 ubiquitination required for DNMT1 recruitment. To test this possibility, we first examined the histone H3 ubiquitination in mouse ESCs. As shown in Figure 5B, H3 mono-ubiquitination was hardly

---

Figure 4. Cell-cycle-dependent acetylation of UHRF1 and the impact of acetylation mutant UHRF1 on DNA methylation maintenance

(A) Representative level of UHRF1 acetylation during the cell cycle in HEK293T cells with stable FLAG-Myc-UHRF1 expression. Cell lysates were collected at different time points after cell-cycle release, and FLAG-tagged UHRF1 was immunoprecipitated with FLAG antibody. The total acetylation and pS652 phosphorylation of UHRF1 in the IP samples were analyzed using acetyl-lysine and pS652-UHRF1 antibodies. FLAG antibody was used to check the UHRF1 loading in the precipitants. The pS652-UHRF1 level was used as a cell-cycle marker, as it peaked at G2/M phase.

(B) HEK293T cells stably transfected with wild-type FLAG-Myc-UHRF1 and transiently transfected with MOF siRNA were synchronized by double thymidine block and followed by cell-cycle release and the same analysis as in (A). The knockdown (KD) efficiency of MOF siRNA is shown in Figure S4A.

(C) Representative immunofluorescence by specific 5mC antibodies in the wild-type and $Uhrf1^{-/-}$ mouse ESCs, as well as $Uhrf1^{-/-}$ mouse ESCs genetically complemented with FLAG-Myc-tagged wild-type UHRF1 (FL) or 3KR or ΔRING mutant UHRF1 constructs. Myc antibodies were employed to detect the exogenous UHRF1. Scale bars, 10 μm. The fluorescence signal of 5mC from ~100 cells was quantified and normalized against the signal in wild-type cells. Data represent relative density value with a standard error from three replicative experiments.

(D) FLAG-Myc-tagged human wild-type UHRF1 and 3KR mutant UHRF1 stably expressed in $Uhrf1^{-/-}$ mouse ESCs were analyzed by western blotting using UHRF1 antibodies. β-Actin was used as the loading control. Two mutant clones and one wild-type clone with UHRF1 expression similar to the endogenous UHRF1 level in wild-type ESCs were selected for the subsequent studies.

(E) Global CG methylation levels of respective portions of the genic regions, measured by RRBS sequencing, in wild-type and $Uhrf1^{-/-}$ mouse ESCs, as well as $Uhrf1^{-/-}$ mouse ESCs genetically complemented with FLAG-Myc-tagged wild-type UHRF1 (hUHRF1) or 3KR (clone #2) UHRF1 constructs. All whisker plots represent the 25th–75th percentiles, with midlines indicating median values. Whiskers extend to the minimum/maximum values of the data, including outliers (black circles).

(F) The DNA methylation status of IAP and LINE1 loci was analyzed by bisulfite sequencing in control ESCs, $Uhrf1^{-/-}$ ESCs, and $Uhrf1^{-/-}$ ESCs stably expressing human wild-type or 3KR mutant UHRF1. The percentage of 5mC was calculated and is shown in two loci.
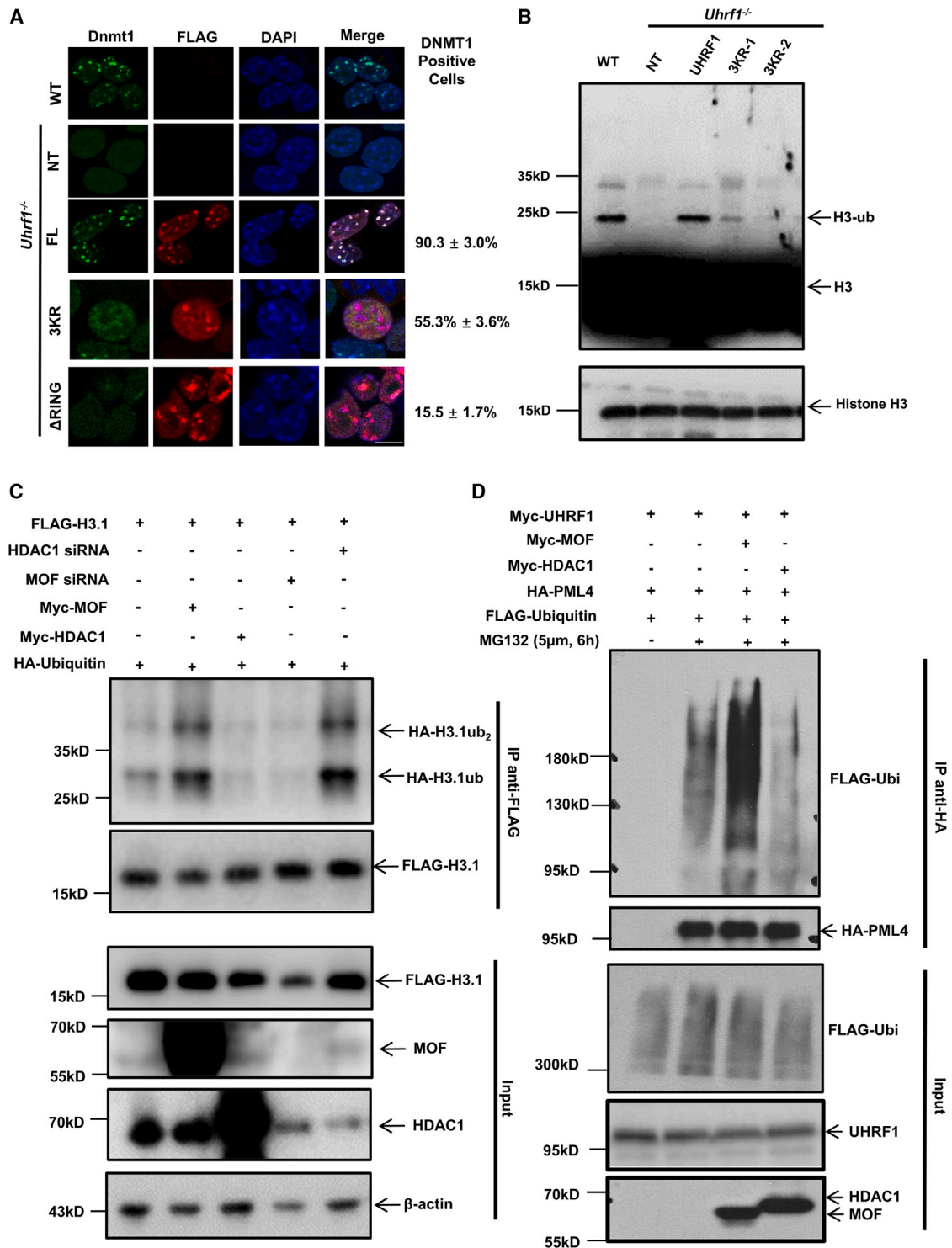
Figure 5. UHRF1 acetylation is required for histone H3 ubiquitination and DNMT1 recruitment

(A) Immunofluorescence analysis of Dnmt1 in *Uhrf1* wild-type ESCs, *Uhrf1*$^{-/-}$ mouse ESCs, and *Uhrf1*$^{-/-}$ mouse ESCs expressing either FLAG-Myc-tagged wild-type UHRF1 or 3KR mutant UHRF1 or ΔRING mutant UHRF1. FLAG antibody was used to detect the exogenous UHRF1. Scale bars, 10 μm. The percentage of cells with normal Dnmt1 foci formation and DNMT1-UHRF1 co-localization, considered as DNMT1-positive cells, was quantified from ~100 cells. Only cells with clear UHRF1 nuclear foci were counted. Numbers represent the percentage of DNMT1-positive cells with a standard error based on three replicative experiments.

(legend continued on next page)

observed in *Uhrf1*$^{-/-}$ ESCs compared to that in wild-type ESCs. The H3 ubiquitination was largely restored in *Uhrf1*$^{-/-}$ ESCs by ectopic human wild-type UHRF1 but not by hypo-acetylated 3KR mutant UHRF1, indicating that hypo-acetylated UHRF1 compromises its E3 ligase activity toward histone H3. A cell-based ubiquitination assay of histone H3.1 in HEK293T cells also confirmed that hypo-acetylated UHRF1 exhibited minimal E3 ligase activity. In HEK293T cells expressing FLAG-H3.1 and hemagglutinin-ubiquitin, ectopic MOF expression or HDAC1 knockdown led to an increase in H3.1 ubiquitination, while ectopic expression of HDAC1 or MOF knockdown significantly reduced the H3.1 ubiquitination (Figure 5C). This is likely a consequence of changes in UHRF1 acetylation mediated by MOF/HDAC1. HDAC family inhibition by TSA or Mof knockdown in wild-type ESCs also affected histone H3 mono-ubiquitination (Figure S7A), consistent with the results from HEK293T cells. However, TSA could not enhance H3 ubiquitination in *Uhrf1*$^{-/-}$ ESCs, suggesting that the effects of MOF and HDAC1 on histone H3 ubiquitination are dependent on UHRF1. Since HDAC1 could also de-acetylate UHRF1 at K490 to enhance UHRF1's binding affinity to hemimethylated DNA, we also stably expressed the K490R/K667R/K668R/K670R (4KR) mutant in *Uhrf1*$^{-/-}$ ESCs. 4KR mutant UHRF1 also failed to restore H3 ubiquitination (Figure S7B), further supporting that MOF-mediated K667/K668/K670 acetylation affects UHRF1's E3 ligase activity. To directly verify that MOF/HDAC1-mediated UHRF1 acetylation results in changes in UHRF1 E3 ligase activity, a well-studied UHRF1 E3 ligase substrate, PML4,[19] was tested for its ubiquitination. As shown in Figure 5D, hyper-acetylation of UHRF1 mediated by MOF significantly enhanced the PML4 poly-ubiquitination, whereas HDAC1-mediated de-acetylation of UHRF1 decreased the PML4 ubiquitination considerably. Consistent with these observations, 3KR hypo-acetylated mutant UHRF1 exhibited reduced E3 ligase activity toward H3.1 and PML4 in 293T compared to wild-type UHRF1 (Figures S7C and S7D), indicating that the acetylation on K670, K667, or K668 is required for efficient E3 ligase activity of UHRF1.

Taken together, these data demonstrated that MOF/HDAC1-mediated UHRF1 acetylation at K670, 667, or 668 modulates UHRF1 E3 ligase activity toward histone H3, whose ubiquitination is required for DNMT1 recruitment during DNA replication and DNA methylation maintenance.

Mof knockdown in mouse ESCs reduces DNA methylation

Since MOF/HDAC1-controlled UHRF1 acetylation could influence UHRF1 E3 ligase function and DNA methylation maintenance during DNA replication, we further explored whether MOF depletion led to a global decrease in DNA methylation. As MOF is an essential regulator for self-renewal and pluripotency in ESCs,[38] only knockdown of Mof in mouse ESCs could be achieved (Figure 6A). As shown in Figures 6A and 6B, the 5mC staining was significantly decreased in two independent Mof knockdown ESC lines compared to that in the wild-type ESCs but was comparable to that in the *Uhrf1*$^{-/-}$ ESCs. In addition, high-throughput RRBS sequencing and bisulfite sequencing analyses of IAP and LINE1 regions in Mof knockdown ESCs also showed reduced global CpG methylation levels compared to that in the wild-type ESCs (Figures 6C and 6D). GO term analysis of the RRBS data also showed that some of the differentiation-related pathways, such as neurogenesis and Wnt signaling, were significantly affected in 3KR mutant cells (Figure S5B), which showed obvious overlap with the analysis in 3KR mutant cells, indicating the DNA methylation defects in MOF knockdown cells were also mediated through UHRF1.

Collectively, these data further confirmed that MOF is critical for DNA methylation maintenance.

DISCUSSION

In this study, we showed that UHRF1 is acetylated and de-acetylated by MOF and HDAC1, respectively. Data obtained from mass spectrometry and mutagenesis experiments indicated that the predominant acetylation site of UHRF1 mediated by MOF is K670, while K667 and K668 could also serve as backup acetylation sites when K670 is mutant or occupied. Acetylation at these sites is critical for DNA methylation maintenance. Abolishing acetylation at these sites in UHRF1 significantly impairs 5mC maintenance in mouse ESCs, leading to reduced global DNA methylation. It is well known that UHRF1 specifically ubiquitinates histone H3 during S phase, which is required for the recruitment of DNMT1.[9] However, the mechanism of how the ubiquitination of histone H3 is precisely regulated remains unknown. In the current study, we demonstrated that the acetylation of UHRF1 in the pre-RING linker region at S phase mediated by MOF could enhance its E3 ligase activity to facilitate the ubiquitination of histone H3, which in turn recruits DNMT1 and maintains the DNA methylation during replication.

The K667/K668/K670 cluster is located in the pre-RING linker region and is known to be subject to extensive post-translational modifications. Previous reports showed that phosphorylation of Ser661 affects UHRF1's nuclear localization.[37] However, our data showed that the hypo-acetylated 3KR mutations at K667/K668/K670 do not affect the nuclear localization (especially heterochromatin) of UHRF1, though those lysine residues are within

---

(B) Representative western blotting from at least three replicative experiments to detect ubiquitinylated histone H3 in wild-type mouse ESCs, *Uhrf1*$^{-/-}$ mouse ESCs, and *Uhrf1*$^{-/-}$ mouse ESCs with ectopic human FLAG-Myc-tagged wild-type UHRF1 or 3KR (two clones) mutant UHRF1. Short exposure of histone H3 as the loading control.

(C) Histone H3.1 ubiquitination in HEK293T cells. The ubiquitination of ectopic FLAG-H3.1 immunoprecipitated from HEK293T cells in the presence of MOF, HDAC1, MOF siRNA, or HDAC1 siRNA was examined by western blotting. Lysates were subjected to IP with FLAG antibody to pull down ectopic histone H3.1, followed by immunoblotting analysis with FLAG and hemagglutinin (HA) antibodies to detect H3.1 and the HA-tagged ubiquitin. The HA-tagged ubiquitin shown in the FLAG IP samples reflects the ubiquitination levels of FLAG-H3.1. Representative western blotting data from at least three replicative experiments are shown.

(D) PML4 ubiquitination in HEK293T cells. HA-PML4, Myc-UHRF1, and FLAG-ubiquitin constructs were transfected into HEK293T cells in the presence or absence of either MOF or HDAC1. The cells were treated with 5 μM MG132 for 6 h before harvest. Cell lysates were subjected to IP with HA antibodies to pull down ectopically expressing wild-type HA-PML4, followed by immunoblotting analysis with HA, FLAG antibody to detect PML4, and the FLAG-tagged ubiquitin. Representative western blotting data from at least three replicative experiments are shown.
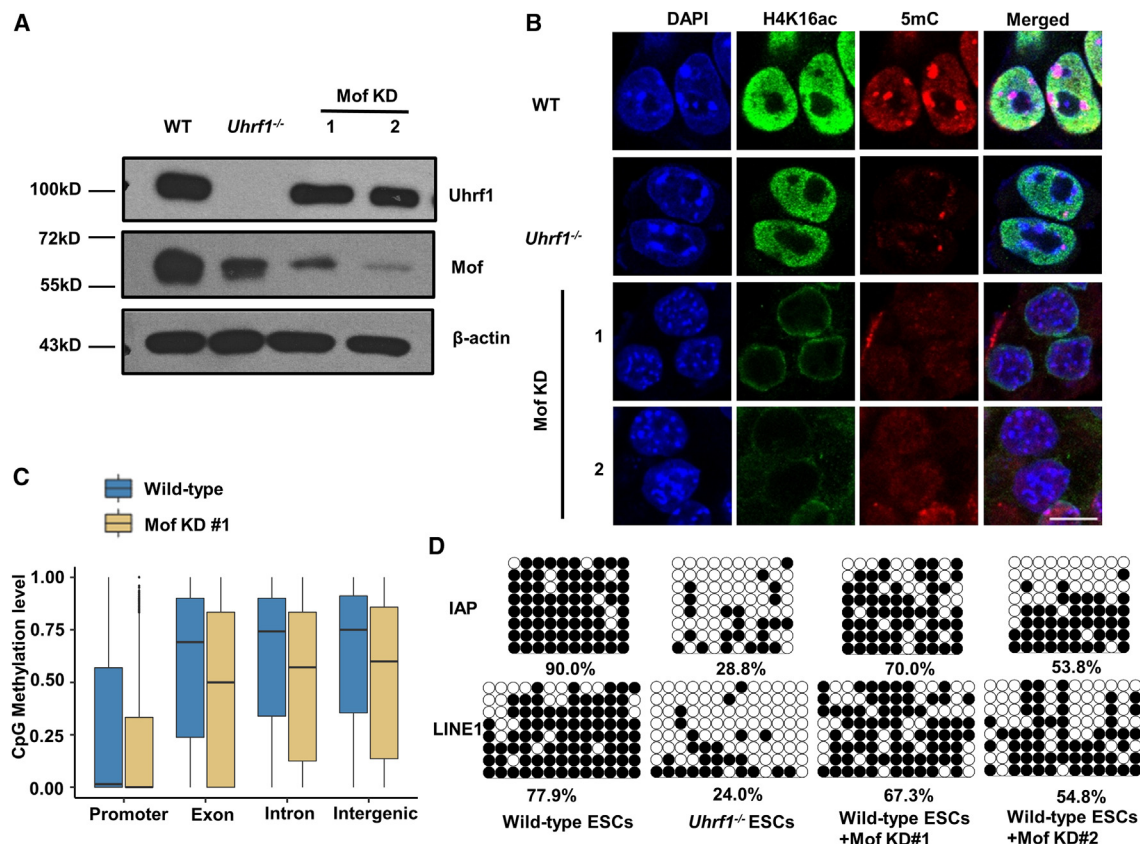
Figure 6. Knocking down Mof in mouse ESCs reduces DNA methylation

(A) Two lines of Mof (KAT8) KD mouse ESCs were generated by stable expression of two different KAT8 short hairpin RNA (shRNA). Cell lysates from mouse ESCs of wild type, *Uhrf1*$^{-/-}$, and Mof KD were subjected to immunoblotting by MOF and UHRF1 antibodies, respectively. β-Actin served as a loading control.

(B) Immunofluorescent staining of 5mC levels in wild-type, *Uhrf1*$^{-/-}$, and Mof KD mouse ESCs. Staining of endogenous H4K16ac to reflect Mof acetyltransferase activity. Scale bars, 10 μm.

(C) Global CpG DNA methylation profiles in different genomic regions, measured by RRBS sequencing, of genomic DNA from wild-type and Mof KD (clone 1) mouse ESCs. All whisker plots represent the 25th–75th percentiles, with midlines indicating median values. Whiskers extend to the minimum/maximum values of the data, including outliers (black circles).

(D) DNA methylation at IAP and LINE1 loci was analyzed by bisulfite sequencing in wild-type, *Uhrf1*$^{-/-}$, and wild-type with stable Mof KD mouse ESCs. The percentage of 5mC at the loci was calculated and is shown in two loci.

a predicted nuclear localization sequence. A recent paper revealed that the de-acetylation of UHRF1 by HDAC1 at K490 could enhance its binding affinity to hemi-methylated DNA and chromatin loading.[28] We showed that the 3KR mutations at K667/K668/K670 did not affect the association of UHRF1 with hemi-methylated DNA. Instead, acetylation of UHRF1 at these residues enhanced its E3 ligase activity toward its known substrates, PML4 and histone H3. Recent studies have identified a spacer region and a polybasic region between the SRA and RING domains in UHRF1.[34,39,40] The conformational changes of these regions could affect the binding affinity of UHRF1 with hemi-methylated DNA and histone H3K9me3 marks. Acetylation of UHRF1 at either K670, K667, or K668 likely causes conformational changes in UHRF1, therefore conferring either increased binding of UHRF1 to its ubiquitination substrates or higher E3 ligase activity.

Though previous studies have performed mass spectrometry to identify UHRF1-interacting proteins,[26,36,41] MOF was not identified in these studies. This could be due to the transient

acetylation process during the S phase, which is in line with the observation of little UHRF1 acetylation in non-synchronized cells. Tip60 has been predicted to acetylate UHRF1 at K646.[33] Despite their similarities in structure and function, MOF and Tip60 do not seem to share similar functions in UHRF1 acetylation. Our cell-based acetylation assay showed that Tip60 is not a major acetyltransferase for UHRF1. Acetyltransferase PCAF and deacetylase HDAC1 were recently reported to mediate the acetylation at K490 in the SRA domain of UHRF1.[28] Acetylation mimic of UHRF1 at K490 attenuates its binding affinity to hemi-methylated DNA and inhibits the inheritance of DNA methylation during DNA replication. Interestingly, knocking down HDAC1 in HCT116 cells does not alter global DNA methylation; instead, it slightly increases DNA methylation,[28] suggesting that de-acetylation of UHRF1 at K490 by HDAC1 is not the critical regulatory mechanism of DNA methylation maintenance during S phase. On the other hand, our data showed that MOF/HDAC1-mediated acetylation of UHRF1 at K667/K668/K670 is critical for DNA

methylation maintenance, as abolishing the acetylation at these sites by 3KR or 4KR (3KR + K490R) hypo-acetylation mutations significantly compromises the inheritance of DNA methylation during DNA replication.

Though the pattern of MOF expression during the cell cycle remains largely unexplored, it has been shown that the histone H4K16 acetylation level, which is mediated by MOF, fluctuates during cell cycle and peaks at S phase.[42] In contrast, the abundance of HDAC1 remains unchanged throughout the cell cycle.[17,28] As MOF depletion causes cells to accumulate at G2/M phase in both human and mouse cells due to S-phase checkpoint deficiency,[43,44] it is conceivable that MOF is critical in DNA replication at S phase. Indeed, our data demonstrated that MOF interacts with UHRF1 and that MOF-mediated acetylation of UHRF1 peaks at S phase of the cell cycle. We showed that MOF acetylates UHRF1 to promote DNA methylation maintenance, revealing an essential positive function of MOF in DNA methylation maintenance during DNA replication.

The protein stability of UHRF1 is regulated by the interaction with USP7 through the polybasic region in UHRF1 and is modulated by phosphorylation on S652[36,40]. This suggests that the post-translational modifications of UHRF1 in the pre-RING linker region are vital for regulating UHRF1 stability. Our data showed that the acetylation of UHRF1 by MOF at K670, K667, or K668 also affects the UHRF1 stability. Upon treatment of 150 μg/mL cycloheximide, a significant reduction in UHRF1 was observed in cells transfected with 3KR mutant UHRF1 compared to that in cells transfected with wild-type UHRF1. (Figure S8A), indicating that the de-acetylation of UHRF1 at K670, K667, or K668 reduces its protein stability. Ectopic expression of MOF in HEK293T cells could also stabilize UHRF1 and prevent it from degradation (Figure S8B). UHRF1 degradation is mediated by E3 ligase β-TrCP1 in a ubiquitination-dependent manner.[24] While 3KR mutant UHRF1 and HDAC1-mediated hypo-acetylated UHRF1 exhibited enhanced poly-ubiquitination of UHRF1, MOF-mediated hyper-acetylated UHRF1 protected UHRF1 from ubiquitination (Figure S9), suggesting that acetylation in UHRF1 maintains its protein stability, in addition to facilitating the E3 ligase activity.

In conclusion, our work revealed K670, K667, and K668 as acetylation sites of UHRF1 and provided a mechanistic explanation for the function of cell-cycle-dependent UHRF1 acetylation in DNA methylation maintenance. We propose a working model for UHRF1 acetylation in DNA replication during the G1/S phase. Upon the recognition of hemi-methylated DNA, UHRF1 is recruited to the nearby histone H3 via interacting H3K9me3 and H3R2 histone marks. Subsequently, acetyltransferase MOF acetylates UHRF1 around the K670 lysine cluster (predominant on K670 and then K667 or K668 when K670 is occupied or mutant) to stabilize UHRF1 and enhance the RING domain E3 ligase activity on histone H3 at K18, K23, and likely other lysine residues as well. The ubiquitinated histone H3 facilitates the recruitment of DNMT1 to the newly synthesized DNA, where DNMT1 will transfer a methyl group to the unmethylated cytosine and maintain the epigenetic information of DNA methylation. When cells exit S phase, deacetylase HDAC1 removes the acetyl group from UHRF1. The de-acetylated UHRF1 is less stable and prone to β-TrCP1-mediated ubiquitination and degradation, which in turn reduces histone H3 ubiquitination and DNMT1 recruitment. Our data provide insights into how MOF-mediated acetylation of UHRF1 regulates epigenetic events, especially the maintenance of global DNA methylation.

Limitations of the study

In the current study, we performed an *in vitro* acetylation assay using purified UHRF1 and MOF (Figure 3A) for identification of the acetylation sites. However, mass spectrometry of endogenous UHRF1 was not included in our study, which may not reveal the *in vivo* scenario of UHRF1 acetylation. Since the acetylation level of UHRF1 is tightly cell-cycle regulated and peaks at G1/S phase, it is possible to detect potential endogenous UHRF1 acetylation sites in S-phase cells. Future studies may synchronize and harvest S-phase cells to perform mass spectrometry for the identification of endogenous UHRF1 acetylation sites. On the other hand, though we have shown that alteration of MOF/HDAC1 expression could affect UHRF1 acetylation as well as DNA methylation, we still could not exclude that 3KR mutations themselves in UHRF1 could also contribute to the DNA methylation defects. In this study, we revealed that the 3KR mutant did not affect UHRF1 chromatin localization, hemi-methylated DNA binding, or DNMT1 and MOF interaction (Figures S2D and S6). Further studies should explore more on whether 3KR mutation will affect UHRF1 function via other mechanisms, such as protein structural changes, in addition to defective E3 ubiquitin ligase activity.

STAR★METHODS

Detailed methods are provided in the online version of this paper and include the following:

- KEY RESOURCES TABLE
- RESOURCE AVAILABILITY
  - Lead contact
  - Materials availability
  - Data and code availability
- EXPERIMENTAL MODEL AND STUDY PARTICIPANT DETAILS
  - Cell lines
- METHOD DETAILS
  - Plasmids used in the study
  - Plasmids transfection, and generation of gene stable expressing ESCs
  - Immunoprecipitation and co-immunoprecipitation
  - Protein purification
  - *In vitro* acetylation assay
  - Immunofluorescence staining
  - Identification of the acetylation sites by mass spectrometry
  - Cell-based ubiquitination assay
  - Bisulfite sequencing
  - Reduced representation bisulfite sequencing (RRBS)
  - Double thymidine block
  - Subcellular fractionation
  - Electrophoretic mobility shift assay
- QUANTIFICATION AND STATISTICAL ANALYSIS

REFERENCES

1. Bronner, C., Krifa, M., and Mousli, M. (2013). Increasing role of UHRF1 in the reading and inheritance of the epigenetic code as well as in tumorogenesis. Biochem. Pharmacol. *86*, 1643–1649. https://doi.org/10.1016/j.bcp.2013.10.002.

2. Bostick, M., Kim, J.K., Estève, P.O., Clark, A., Pradhan, S., and Jacobsen, S.E. (2007). UHRF1 plays a role in maintaining DNA methylation in mammalian cells. Science *317*, 1760–1764. https://doi.org/10.1126/science.1147939.

3. Sharif, J., Muto, M., Takebayashi, S.i., Suetake, I., Iwamatsu, A., Endo, T.A., Shinga, J., Mizutani-Koseki, Y., Toyoda, T., Okamura, K., et al. (2007). The SRA protein Np95 mediates epigenetic inheritance by recruiting Dnmt1 to methylated DNA. Nature *450*, 908–912. https://doi.org/10.1038/nature06397.

4. Ferry, L., Fournier, A., Tsusaka, T., Adelmant, G., Shimazu, T., Matano, S., Kirsh, O., Amouroux, R., Dohmae, N., Suzuki, T., et al. (2017). Methylation of DNA Ligase 1 by G9a/GLP Recruits UHRF1 to Replicating DNA and Regulates DNA Methylation. Mol. Cell *67*, 550–565.e5. https://doi.org/10.1016/j.molcel.2017.07.012.

5. Miura, M., Watanabe, H., Sasaki, T., Tatsumi, K., and Muto, M. (2001). Dynamic changes in subnuclear NP95 location during the cell cycle and its spatial relationship with DNA replication foci. Exp. Cell Res. *263*, 202–208. https://doi.org/10.1006/excr.2000.5115.

6. Liu, X., Gao, Q., Li, P., Zhao, Q., Zhang, J., Li, J., Koseki, H., and Wong, J. (2013). UHRF1 targets DNMT1 for DNA methylation through cooperative binding of hemi-methylated DNA and methylated H3K9. Nat. Commun. *4*, 1563. https://doi.org/10.1038/ncomms2562.

7. Zhao, Q., Zhang, J., Chen, R., Wang, L., Li, B., Cheng, H., Duan, X., Zhu, H., Wei, W., Li, J., et al. (2016). Dissecting the precise role of H3K9 methylation in crosstalk with DNA maintenance methylation in mammals. Nat. Commun. *7*, 12464. https://doi.org/10.1038/ncomms12464.

8. Veland, N., Hardikar, S., Zhong, Y., Gayatri, S., Dan, J., Strahl, B.D., Rothbart, S.B., Bedford, M.T., and Chen, T. (2017). The Arginine Methyltransferase PRMT6 Regulates DNA Methylation and Contributes to Global DNA Hypomethylation in Cancer. Cell Rep. *21*, 3390–3397. https://doi.org/10.1016/j.celrep.2017.11.082.

9. Nishiyama, A., Yamaguchi, L., Sharif, J., Johmura, Y., Kawamura, T., Nakanishi, K., Shimamura, S., Arita, K., Kodama, T., Ishikawa, F., et al. (2013). Uhrf1-dependent H3K23 ubiquitylation couples maintenance DNA methylation and replication. Nature *502*, 249–253. https://doi.org/10.1038/nature12488.

10. Qin, W., Wolf, P., Liu, N., Link, S., Smets, M., La Mastra, F., Forné, I., Pichler, G., Hörl, D., Fellinger, K., et al. (2015). DNA methylation requires a DNMT1 ubiquitin interacting motif (UIM) and histone ubiquitination. Cell Res. *25*, 911–929. https://doi.org/10.1038/cr.2015.72.

11. Ishiyama, S., Nishiyama, A., Saeki, Y., Moritsugu, K., Morimoto, D., Yamaguchi, L., Arai, N., Matsumura, R., Kawakami, T., Mishima, Y., et al. (2017). Structure of the Dnmt1 Reader Module Complexed with a Unique Two-Mono-Ubiquitin Mark on Histone H3 Reveals the Basis for DNA Methylation Maintenance. Mol. Cell *68*, 350–360.e7. https://doi.org/10.1016/j.molcel.2017.09.037.

12. Li, T., Wang, L., Du, Y., Xie, S., Yang, X., Lian, F., Zhou, Z., and Qian, C. (2018). Structural and mechanistic insights into UHRF1-mediated DNMT1 activation in the maintenance DNA methylation. Nucleic Acids Res. *46*, 3218–3231. https://doi.org/10.1093/nar/gky104.

13. Dai, C., Shi, D., and Gu, W. (2013). Negative regulation of the acetyltransferase TIP60-p53 interplay by UHRF1 (ubiquitin-like with PHD and RING finger domains 1). J. Biol. Chem. *288*, 19581–19592. https://doi.org/10.1074/jbc.M113.476606.

14. Ma, J., Peng, J., Mo, R., Ma, S., Wang, J., Zang, L., Li, W., and Fan, J. (2015). Ubiquitin E3 ligase UHRF1 regulates p53 ubiquitination and p53-dependent cell apoptosis in clear cell Renal Cell Carcinoma. Biochem. Biophys. Res. Commun. *464*, 147–153. https://doi.org/10.1016/j.bbrc.2015.06.104.

15. Nishiyama, A., Mulholland, C.B., Bultmann, S., Kori, S., Endo, A., Saeki, Y., Qin, W., Trummer, C., Chiba, Y., Yokoyama, H., et al. (2020). Two distinct modes of DNMT1 recruitment ensure stable maintenance DNA methylation. Nat. Commun. *11*, 1222. https://doi.org/10.1038/s41467-020-15006-4.

16. Karg, E., Smets, M., Ryan, J., Forné, I., Qin, W., Mulholland, C.B., Kalideris, G., Imhof, A., Bultmann, S., and Leonhardt, H. (2017). Ubiquitome Analysis Reveals PCNA-Associated Factor 15 (PAF15) as a Specific Ubiquitination Target of UHRF1 in Embryonic Stem Cells. J. Mol. Biol. *429*, 3814–3824. https://doi.org/10.1016/j.jmb.2017.10.014.

17. Du, Z., Song, J., Wang, Y., Zhao, Y., Guda, K., Yang, S., Kao, H.Y., Xu, Y., Willis, J., Markowitz, S.D., et al. (2010). DNMT1 stability is regulated by proteins coordinating deubiquitination and acetylation-driven ubiquitination. Sci. Signal. *3*, ra80. https://doi.org/10.1126/scisignal.2001462.

18. De Vos, M., El Ramy, R., Quénet, D., Wolf, P., Spada, F., Magroun, N., Babbio, F., Schreiber, V., Leonhardt, H., Bonapace, I.M., and Dantzer, F. (2014). Poly(ADP-ribose) polymerase 1 (PARP1) associates with E3 ubiquitin-protein ligase UHRF1 and modulates UHRF1 biological functions. J. Biol. Chem. *289*, 16223–16238. https://doi.org/10.1074/jbc.M113.527424.

19. Guan, D., Factor, D., Liu, Y., Wang, Z., and Kao, H.Y. (2013). The epigenetic regulator UHRF1 promotes ubiquitination-mediated degradation of the tumor-suppressor protein promyelocytic leukemia protein. Oncogene *32*, 3819–3828. https://doi.org/10.1038/onc.2012.406.

20. Jia, Y., Li, P., Fang, L., Zhu, H., Xu, L., Cheng, H., Zhang, J., Li, F., Feng, Y., Li, Y., et al. (2016). Negative regulation of DNMT3A de novo DNA methylation by frequently overexpressed UHRF family proteins as a mechanism for widespread DNA hypomethylation in cancer. Cell Discov. *2*, 16007. https://doi.org/10.1038/celldisc.2016.7.

21. Trotzier, M.A., Bronner, C., Bathami, K., Mathieu, E., Abbady, A.Q., Jeanblanc, M., Muller, C.D., Rochette-Egly, C., and Mousli, M. (2004). Phosphorylation of ICBP90 by protein kinase A enhances topoisomerase IIalpha expression. Biochem. Biophys. Res. Commun. *319*, 590–595. https://doi.org/10.1016/j.bbrc.2004.05.028.

22. Arita, K., Isogai, S., Oda, T., Unoki, M., Sugita, K., Sekiyama, N., Kuwata, K., Hamamoto, R., Tochio, H., Sato, M., et al. (2012). Recognition of modification status on a histone H3 tail by linked histone reader modules of the epigenetic regulator UHRF1. Proc. Natl. Acad. Sci. USA 109, 12950–12955. https://doi.org/10.1073/pnas.1203701109.

23. Yang, J., Liu, K., Yang, J., Jin, B., Chen, H., Zhan, X., Li, Z., Wang, L., Shen, X., Li, M., et al. (2017). PIM1 induces cellular senescence through phosphorylation of UHRF1 at Ser311. Oncogene 36, 4828–4842. https://doi.org/10.1038/onc.2017.96.

24. Chen, H., Ma, H., Inuzuka, H., Diao, J., Lan, F., Shi, Y.G., Wei, W., and Shi, Y. (2013). DNA Damage Regulates UHRF1 Stability via the SCFβ-TrCP E3 Ligase. Mol. Cell Biol. 33, 1139–1148. https://doi.org/10.1128/mcb.01191-12.

25. Felle, M., Joppien, S., Németh, A., Diermeier, S., Thalhammer, V., Dobner, T., Kremmer, E., Kappler, R., and Längst, G. (2011). The USP7/Dnmt1 complex stimulates the DNA methylation activity of Dnmt1 and regulates the stability of UHRF1. Nucleic Acids Res. 39, 8355–8365. https://doi.org/10.1093/nar/gkr528.

26. Hahm, J.Y., Kim, J.Y., Park, J.W., Kang, J.Y., Kim, K.B., Kim, S.R., Cho, H., and Seo, S.B. (2019). Methylation of UHRF1 by SET7 is essential for DNA double-strand break repair. Nucleic Acids Res. 47, 184–196. https://doi.org/10.1093/nar/gky975.

27. Achour, M., Fuhrmann, G., Alhosin, M., Rondé, P., Chataigneau, T., Mousli, M., Schini-Kerth, V.B., and Bronner, C. (2009). UHRF1 recruits the histone acetyltransferase Tip60 and controls its expression and activity. Biochem. Biophys. Res. Commun. 390, 523–528. https://doi.org/10.1016/j.bbrc.2009.09.131.

28. Hahm, J.Y., Park, J.W., Kang, J.-Y., Park, J., Kim, C.-H., Kim, J.-Y., Ha, N.-C., Kim, J.-W., and Seo, S.-B. (2020). Acetylation of UHRF1 Regulates Hemi-methylated DNA Binding and Maintenance of Genome-wide DNA Methylation. Cell Rep. 32, 107958. https://doi.org/10.1016/j.celrep.2020.107958.

29. Avvakumov, N., and Côté, J. (2007). The MYST family of histone acetyltransferases and their intimate links to cancer. Oncogene 26, 5395–5407. https://doi.org/10.1038/sj.onc.1210608.

30. Bone, J.R., Lavender, J., Richman, R., Palmer, M.J., Turner, B.M., and Kuroda, M.I. (1994). Acetylated histone H4 on the male X chromosome is associated with dosage compensation in Drosophila. Genes Dev. 8, 96–104.

31. Sykes, S.M., Mellert, H.S., Holbert, M.A., Li, K., Marmorstein, R., Lane, W.S., and McMahon, S.B. (2006). Acetylation of the p53 DNA-binding domain regulates apoptosis induction. Mol. Cell 24, 841–851. https://doi.org/10.1016/j.molcel.2006.11.026.

32. Candido, E.P., Reeves, R., and Davie, J.R. (1978). Sodium butyrate inhibits histone deacetylation in cultured cells. Cell 14, 105–113.

33. Choudhary, C., Kumar, C., Gnad, F., Nielsen, M.L., Rehman, M., Walther, T.C., Olsen, J.V., and Mann, M. (2009). Lysine acetylation targets protein complexes and co-regulates major cellular functions. Science 325, 834–840. https://doi.org/10.1126/science.1175371.

34. Gelato, K.A., Tauber, M., Ong, M.S., Winter, S., Hiragami-Hamada, K., Sindlinger, J., Lemak, A., Bultsma, Y., Houliston, S., Schwarzer, D., et al. (2014). Accessibility of different histone H3-binding domains of UHRF1 is allosterically regulated by phosphatidylinositol 5-phosphate. Mol. Cell 54, 905–919. https://doi.org/10.1016/j.molcel.2014.04.004.

35. Jenkins, Y., Markovtsov, V., Lang, W., Sharma, P., Pearsall, D., Warner, J., Franci, C., Huang, B., Huang, J., Yam, G.C., et al. (2005). Critical role of the ubiquitin ligase activity of UHRF1, a nuclear RING finger protein, in tumor cell growth. Mol. Biol. Cell 16, 5621–5629. https://doi.org/10.1091/mbc.E05-03-0194.

36. Ma, H., Chen, H., Guo, X., Wang, Z., Sowa, M.E., Zheng, L., Hu, S., Zeng, P., Guo, R., Diao, J., et al. (2012). M phase phosphorylation of the epigenetic regulator UHRF1 regulates its physical association with the deubiquitylase USP7 and stability. Proc. Natl. Acad. Sci. USA 109, 4828–4833. https://doi.org/10.1073/pnas.1116349109.

37. Chu, J., Loughlin, E.A., Gaur, N.A., SenBanerjee, S., Jacob, V., Monson, C., Kent, B., Oranu, A., Ding, Y., Ukomadu, C., and Sadler, K.C. (2012). UHRF1 phosphorylation by cyclin A2/cyclin-dependent kinase 2 is required for zebrafish embryogenesis. Mol. Biol. Cell 23, 59–70. https://doi.org/10.1091/mbc.E11-06-0487.

38. Li, X., Li, L., Pandey, R., Byun, J.S., Gardner, K., Qin, Z., and Dou, Y. (2012). The histone acetyltransferase MOF is a key regulator of the embryonic stem cell core transcriptional network. Cell Stem Cell 11, 163–178. https://doi.org/10.1016/j.stem.2012.04.023.

39. Fang, J., Cheng, J., Wang, J., Zhang, Q., Liu, M., Gong, R., Wang, P., Zhang, X., Feng, Y., Lan, W., et al. (2016). Hemi-methylated DNA opens a closed conformation of UHRF1 to facilitate its histone recognition. Nat. Commun. 7, 11197. https://doi.org/10.1038/ncomms11197.

40. Zhang, Z.M., Rothbart, S.B., Allison, D.F., Cai, Q., Harrison, J.S., Li, L., Wang, Y., Strahl, B.D., Wang, G.G., and Song, J. (2015). An Allosteric Interaction Links USP7 to Deubiquitination and Chromatin Targeting of UHRF1. Cell Rep. 12, 1400–1406. https://doi.org/10.1016/j.celrep.2015.07.046.

41. Kim, K.-Y., Tanaka, Y., Su, J., Cakir, B., Xiang, Y., Patterson, B., Ding, J., Jung, Y.-W., Kim, J.-H., Hysolli, E., et al. (2018). Uhrf1 regulates active transcriptional marks at bivalent domains in pluripotent stem cells through Setd1a. Nat. Commun. 9, 2583. https://doi.org/10.1038/s41467-018-04818-0.

42. Rice, J.C., Nishioka, K., Sarma, K., Steward, R., Reinberg, D., and Allis, C.D. (2002). Mitotic-specific methylation of histone H4 Lys 20 follows increased PR-Set7 expression and its localization to mitotic chromosomes. Genes Dev. 16, 2225–2230. https://doi.org/10.1101/gad.1014902.

43. Sharma, G.G., So, S., Gupta, A., Kumar, R., Cayrou, C., Avvakumov, N., Bhadra, U., Pandita, R.K., Porteus, M.H., Chen, D.J., et al. (2010). MOF and histone H4 acetylation at lysine 16 are critical for DNA damage response and double-strand break repair. Mol. Cell Biol. 30, 3582–3595. https://doi.org/10.1128/mcb.01476-09.

44. Li, X., Corsa, C.A.S., Pan, P.W., Wu, L., Ferguson, D., Yu, X., Min, J., and Dou, Y. (2010). MOF and H4 K16 acetylation play important roles in DNA damage repair by modulating recruitment of DNA damage repair protein Mdc1. Mol. Cell Biol. 30, 5335–5347. https://doi.org/10.1128/mcb.00350-10.

45. Lu, L.Y., Kuang, H., Korakavi, G., and Yu, X. (2015). Topoisomerase II regulates the maintenance of DNA methylation. J. Biol. Chem. 290, 851–860. https://doi.org/10.1074/jbc.M114.611509.

46. Martínez-Balbás, M.A., Bauer, U.M., Nielsen, S.J., Brehm, A., and Kouzarides, T. (2000). Regulation of E2F1 activity by acetylation. EMBO J. 19, 662–671. https://doi.org/10.1093/emboj/19.4.662.

47. Kamitani, T., Kito, K., Nguyen, H.P., and Yeh, E.T. (1997). Characterization of NEDD8, a developmentally down-regulated ubiquitin-like protein. J. Biol. Chem. 272, 28557–28562. https://doi.org/10.1074/jbc.272.45.28557.

48. Cox, J., and Mann, M. (2008). MaxQuant enables high peptide identification rates, individualized p.p.b.-range mass accuracies and proteome-wide protein quantification. Nat. Biotechnol. 26, 1367–1372. https://doi.org/10.1038/nbt.1511.

49. Kumaki, Y., Oda, M., and Okano, M. (2008). QUMA: quantification tool for methylation analysis. Nucleic Acids Res. 36, W170–W175. https://doi.org/10.1093/nar/gkn294.

50. Xi, Y., and Li, W. (2009). BSMAP: whole genome bisulfite sequence MAPping program. BMC Bioinf. 10, 232. https://doi.org/10.1186/1471-2105-10-232.

51. Jühling, F., Kretzmer, H., Bernhart, S.H., Otto, C., Stadler, P.F., and Hoffmann, S. (2016). metilene: fast and sensitive calling of differentially methylated regions from bisulfite sequencing data. Genome Res. 26, 256–262. https://doi.org/10.1101/gr.196394.115.

52. Wang, J., Xia, Y., Li, L., Gong, D., Yao, Y., Luo, H., Lu, H., Yi, N., Wu, H., Zhang, X., et al. (2013). Double restriction-enzyme digestion improves the coverage and accuracy of genome-wide CpG methylation profiling by reduced representation bisulfite sequencing. BMC Genom. 14, 11. https://doi.org/10.1186/1471-2164-14-11.

STAR★METHODS

KEY RESOURCES TABLE

REAGENT or RESOURCE	SOURCE	IDENTIFIER
Antibodies		
Anti-5-mC	Diagenode	Cat#C15200081, RRID:AB_2572207
Anti-acetyl-Lysine	Millipore	Cat#AB3879, RRID:AB_570574
Anti-acetyl-Histone H4, Lys16	Millipore	Cat#05–1232, RRID:AB_1587137
Anti-*c*-Myc	Santa Cruz	Cat#sc-40, RRID:AB_627268
Anti-*c*-Myc	Sigma-Aldrich	Cat#C3956, RRID:AB_439680
Anti-DNMT1	Santa Cruz	Cat#sc-20701, RRID:AB_2293064
Anti-FLAG-tag (mouse)	Sigma-Aldrich	Cat#F1804, RRID:AB_262044
Anti-FLAG-tag (rabbit)	Sigma-Aldrich	Cat#F7425, RRID:AB_439687
Anti-HA-tag (mouse)	Santa Cruz	Cat#sc-7392, RRID:AB_627809
Anti-HA-tag (rabbit)	Santa Cruz	Cat#sc-805, RRID:AB_631618
Anti-GST-tag	Abcam	Cat#ab9085, RRID:AB_306993
Anti-HDAC1	Santa Cruz	Cat#sc-8410, RRID:AB_627703
Anti-Histone H3	Cell Signaling	Cat#3638, RRID:AB_1642229
Anti-MOF	Abcam	Cat#ab200660, RRID:AB_2891127
Anti-Ubiquitin	Cell Signaling	Cat#3936, RRID:AB_331292
Anti-pS652-UHRF1	Prof. Yang Shi[36]	N/A
Anti-β-actin	Sigma-Aldrich	Cat#A5316, RRID:AB_476743
Anti-GAPDH	Abcam	Cat#ab9484, RRID:AB_307274
Goat Anti-Mouse IgG (H + L)	ThermoFisher	Cat#31430, RRID:AB_228307
Rabbit Anti-Goat IgG (H + L)	ThermoFisher	Cat#31402, RRID:AB_228395
Alexa Fluor 568 goat anti-mouse IgG1	Invitrogen	Cat#A21124, RRID:AB_141611
Alexa Fluor 488 donkey anti-rabbit IgG (H + L)	Invitrogen	Cat#A21206, RRID:AB_2535792
Bacterial and virus strains		
Rosetta (DE3) Competent Cells	Sigma-Aldrich	Cat#70954
Chemicals, peptides, and recombinant proteins		
Gelatin	Sigma-Aldrich	Cat#G1890
DMEM (high glucose)	Gibco	Cat#11965
ES-fetal bovine serum	Gibco	Cat#16141079
Fetal bovine serum	Gibco	Cat#10270106
Leukemia Inhibitory Factor	Millipore	Cat#ESG1107
GlutaMAX Supplement	Life Technologies	Cat#35050
Sodium Pyruvate	Life Technologies	Cat#11360
2-Mercaptoethanol	Life Technologies	Cat#31350
Lipofectamine 3000	Invitrogen	Cat#L3000015
X-tremeGene HP DNA Transfection Reagent	Roche	Cat#6366236001
Lipofectamine RNAiMAX	Invitrogen	Cat#13778075
Protein G Agarose	Invitrogen	Cat#15920-010
Anti-FLAG M2 Magnetic Beads	Sigma-Aldrich	Cat#M8823
HA affinity gel	ThermoFisher	Cat#26182
Hygromycin B	Gibco	Cat#10687010
Glutathione agarose beads	ThermoFisher	Cat#16101
2x Laemmli Sample Buffer	Bio-Rad	Cat#1610737
Protease inhibitor cocktail	Roche	Cat#04693132001
Triton X-100	Sigma-Aldrich	Cat#T8787

(Continued on next page)

Continued

REAGENT or RESOURCE	SOURCE	IDENTIFIER
Slow Fade Gold antifade reagent with DAPI	Invitrogen	Cat#S36938
MG132	Abccam	Cat#ab141003
Nonidet P-40 (NP40)	Calbiochem	Cat#492015
N-ethyl maleimide	Sigma-Aldrich	Cat#128287
Thymidine	Sigma-Aldrich	Cat#T9250
Critical commercial assays		
QuikChange II XL Site-Directed Mutagenesis Kit	Agilent Technologies	Cat# 200522
TIANamp Genomic DNA Kit	Tiangen	Cat#DP304
EpiTect Bisulfite kit	Qiagen	Cat#59104
Deposited data		
Reduced representation bisulfite sequencing (RRBS) data	This study	GEO: GSE225947
Mass spectrometry data	This study	PRIDE: PXD040426
Experimental models: Cell lines		
Mouse ES cells (RRZ054)	Dr. Lin-Yu Lu[45]	N/A
HeLa	ATCC	CCL-2
HEK293T	ATCC	CRL-3216
Oligonucleotides		
MOF siRNA	Santa Cruz	Cat# sc-37129
HDAC1 siRNA	Santa Cruz	Cat# sc-29343
Mutagenesis primers of UHRF1	This paper	See Table S1 for a list of Mutagenesis Primers
Cloning primers of MOF shRNA and FLAG-Ubiquitin plasmids	This paper	See Table S1 for a list of cloning Primers
BS-seq Primer: IAP F: ATTTTGTTGATTAAATAAATTATTATTGGG	This paper	N/A
BS-seq Primer: IAP R: TAAAACATATCCTCTAATCATTTCTACTCA	This paper	N/A
BS-seq Primer: LINE1 F: TTATTTTGATAGTAGAGTT	This paper	N/A
BS-seq Primer: LINE1 R: CAAACCAAACTCCTAACAA	This paper	N/A
Forward hemi-mCpG probes: TTGCACTCTC CTCCXGGAAGTCCCAGCTTC, X = 5-methyldeoxycytosine	This paper	N/A
Reverse hemi-mCpG probes: GAAGCTGGGA CTTCCGGGAGGAGAGTGCAA	This paper	N/A
Recombinant DNA		
FLAG-Myc-UHRF1	Origene	RC217766
FLAG-Myc-DNMT1	Origene	RC226414
Myc-UHRF1 on pCMV-Myc-N vector (full-length and domain deleted)	This paper	N/A
pcDNA3.1-FLAG-Tip60	This paper	N/A
pCMV-Myc-His-MOF and other MOF plasmids	This paper	N/A
pCMV3-C-Myc-HBO1	Sino Biological Inc.	Cat: HG15000-CM
pCMV3-C-Myc-HDAC1	Sino Biological Inc.	Cat: HG11486-CM
pcDNA3.1-HA-p300	This paper	N/A
pCMV-sport2-FLAG-GCN5	Sharon Dent[46]	RRID:Addgene_23098
HA-Ubiquitin	Edward Yeh[47]	RRID:Addgene_18712
pCMX-PML4-HA	This paper	N/A
The β-TrCP1-HA	This paper	N/A
pcDNA3.1-Histone H3.1-FLAG	This paper	N/A
Mof (KAT8) mouse shRNA plasmids (sh19)	This paper	N/A
Mof (KAT8) mouse shRNA plasmids (sh21)	This paper	N/A

(Continued on next page)

Continued

REAGENT or RESOURCE	SOURCE	IDENTIFIER
pcDNA3.1-FLAG-Ubi	This paper	N/A
FLAG-Myc-UHRF1 (domain-deleted, domain-swapped, and point mutants)	This paper	N/A
GST-tagged UHRF1 and MOF plasmids	This paper	N/A
pGEM-T vector	Promega	Cat#A3600
Software and algorithms		
Maxquant (version 2.0.3.0)	Jürgen Cox[48]	https://www.maxquant.org/maxquant/
QUMA	Masaki Okano[49]	http://quma.cdb.riken.jp/
Trim Galore (version: 0.5.0)	Felix Krueger	https://www.bioinformatics.babraham.ac.uk/projects/trim_galore/
BSMAP (version 2.73)	Wei Li[50]	http://code.google.com/p/bsmap/
metilene	Frank Jühling[51]	http://legacy.bioinf.uni-leipzig.de/Software/metilene/
R (version 4.3.1)	The R Foundation	https://www.r-project.org/
GraphPad Prism	GraphPad	https://www.graphpad.com

RESOURCE AVAILABILITY

Lead contact
Further information and requests for resources and reagents should be directed to and will be fulfilled by the lead contact, Zhongjun Zhou (zhongjun@hku.hk).

Materials availability
All unique/stable reagents and materials generated in this study are available from the lead contact without restriction.

Data and code availability
- Reduced representation bisulfite sequencing (RRBS) data have been deposited at Gene Expression Omnibus (GEO) and are publicly available as of the date of publication. The accession number is listed in the key resources table.
- The mass spectrometry data have been deposited at Proteomics Identification Database (PRIDE) and are publicly available as of the date of publication. The accession number is listed in the key resources table.
- This paper does not report original code.
- Any additional information required to reanalyze the data reported in this paper is available from the lead contact upon request.

EXPERIMENTAL MODEL AND STUDY PARTICIPANT DETAILS

Cell lines
Secondary cell lines, HEK293T, and HeLa cells were obtained from American Type Culture Collection (ATCC). Both cells were cultured in Dulbecco's modified Eagle medium (Gibco, 11965) with 10% fetal bovine serum (Gibco, Cat: 10270106), maintained in a 37°C incubator with 5% CO2, and passaged every two days.

Mouse WT ESCs, *Uhrf1*$^{-/-}$ ESCs (RRZ054) were kindly provided by Dr. Lin-Yu Lu,[45] and were cultured on 0.1% gelatin (Sigma) coated dishes in DMEM (high glucose, Gibco, 11965), supplemented with 15% ES-fetal bovine serum (Gibco, 16141-079), 100 units/mL Leukemia Inhibitory Factor (Millipore, ESG1107), GlutaMAX Supplement (Life Technologies, 35050), Sodium Pyruvate (Life Technologies, 11360), and 2-Mercaptoethanol (Life Technologies, 31350), maintained in a 37°C incubator with 5% CO$_2$, and passaged every two days.

METHOD DETAILS

Plasmids used in the study
The FLAG-Myc-UHRF1 and FLAG-Myc-DNMT1 on pCMV6-Entry vector were purchased from Origene (RC217766 and RC226414). The Myc-tagged full-length and domain deleted UHRF1 on pCMV-myc-N vector were gifts from Professor Gu Wei (Harvard University). The pcDNA3.1-FLAG-Tip60 constructs were gifts from Dr. Edward Seto (H.Lee Moffitt Cancer Center and Research Institute), and the pCMV-Myc-His-MOF and other MOF constructs were obtained from Dr. Maggie Chow (The University of Hong Kong). The pCMV3-C-Myc-HBO1 (Cat: HG15000-CM) and pCMV3-C-Myc-HDAC1 (Cat: HG11486-CM) plasmids were purchased from Sino

Biological Inc., whereas the pcDNA3.1-HA-p300 construct was obtained from Dr. Baohua Liu (Shenzhen University). The pCMV-sport2-FLAG-GCN5 (#23098) and HA-Ubiquitin (#18712) plasmids were obtained from Addgene. pCMX-PML4-HA plasmids were gifts from Dr. H-Y Kao (Case Western Reserve University). The β-TrCP1-HA plasmids were gifts from Dr. Yang Shi (Fudan University Medical School), and pcDNA3.1-Histone H3.1-FLAG plasmids were gifts from Dr. Kui Ming Chan (City University of Hong Kong). Mof (KAT8) mouse shRNA plasmids were generated by annealing KAT8sh19F/KAT8sh19R or KAT8sh21F/KAT8sh21R oligos and inserted into PiggyBac vectors with CAG promoter. The pcDNA3.1-FLAG-Ubi plasmids were generated by PCR cloning using FLAG-Ubi-For/Ubi-Rev primers and inserted into the pcDNA3.1 plasmid. FLAG-Myc-UHRF1 domain-deleted, domain-swapped, and point mutants were generated using the QuikChange site-directed mutagenesis kit (Stratagene). The presence of appropriate mutations was confirmed by DNA sequencing. FLAG-Myc-tagged wild-type human UHRF1 cDNA, as well as their mutants, were re-constructed into PiggyBac vectors with CAG promoter for expression in ES cells.

Plasmids transfection, and generation of gene stable expressing ESCs

Plasmids containing FLAG-Myc-tagged human wild-type UHRF1, various domain deleted UHRF1, point mutated UHRF1, or Mof knockdown shRNA (all in PiggyBac vectors with CAG promoter) were transfected to *Uhrf1* knockout ES cells or HEK293T cells using Lipofectamine 3000 (Invitrogen, L3000015) according to the manufacturer's protocol. Cells were selected by Hygromycin, and single colonies were picked to obtain cells with homogeneous gene expression levels. The transient transfection of secondary cells was performed using X-tremeGene HP DNA Transfection Reagent (Roche). MOF siRNA (Santa Cruz, sc-37129) and HDAC1 siRNA (Santa Cruz, sc-29343) transfection was done by Lipofectamine RNAiMAX (ThermoFisher).

Immunoprecipitation and co-immunoprecipitation

For the immunoprecipitation of specific proteins from cells, one 10 cm dish of 90% confluent cells was collected. The cells were first washed twice with ice-cold PBS and scraped down in 1 mL of RIPA buffer. After incubation on ice for 15 min, the cell lysate was sonicated twice for 15 s. The lysate was centrifuged at 13,000 rpm for 10 min at 4°C. The supernatant was transferred to a new 1.5 mL Eppendorf tube. 50 μL of the lysate was collected as input. After pre-clearing, the supernatant was mixed with 2 μg of the primary antibodies and 40 μL Protein G Agarose (or FLAG-M2/HA affinity gel). The reaction was incubated by shaking at 4°C overnight. On the next day, the agarose beads conjugated to the antibodies and protein complex were precipitated, followed by three washes with RIPA buffer (containing 500 mM NaCl or otherwise specified). The beads were mixed with 50 μL 2x Laemmli Sample Buffer and boiled for 10 min. The supernatant was collected after centrifugation at 13,000 rpm for 2 min and subject to Western blotting analysis.

Protein purification

DNA sequence encoding human full-length MOF (aa: 1–458), full-length, and different domain-deleted UHRF1 was sub-cloned into N-terminal GST-tagged pGEX-6P-1 vector. The plasmids were transformed into Escherichia coli strain Rosetta DE3 (Novagen), and the expression of recombinant proteins was induced by 0.3 mM IPTG at 16°C overnight. The bacteria were collected by centrifugation at 4,000 rpm for 30 min and resuspended in Buffer A (20 mM Tris, 150 mM NaCl, pH 7.4). After brief sonication (in the presence of protease inhibitor cocktail), the supernatant containing the recombinant proteins was collected by centrifugation at 18, 000 rpm for 40 min at 4°C. Purification of recombinant proteins was achieved by incubating the supernatant with glutathione agarose beads (Thermo Scientific, Cat: #16101) at 4°C for 1 h. The beads were then washed three times, and the recombinant proteins were eluted in Buffer B (20 mM Tris, 150 mM NaCl, 50 mM glutathione pH 7.4) at 4°C for 30 min.

In vitro acetylation assay

Briefly, about 2 μg of recombinant human MOF protein and 500 ng recombinant human UHRF1 protein were incubated in 50 μL acetyltransferase assay buffer (50 mM Tris-HCl, pH 8.0, 10% glycerol, 0.1 mM EDTA and 1 mM dithiothreitol) in the presence of 20 μM acetyl CoA at 30°C for 2 h. The reaction mixture was then applied to SDS-PAGE and immunoblotted with an anti-acetyl lysine antibody.

Immunofluorescence staining

For immunofluorescence, ESCs or other cell lines were fixed with 4% paraformaldehyde in PBS for 15 min at 25°C, followed by treatment with 0.1%Triton X-100 (Sigma-Aldrich) in PBS for 10 min at 25°C. Cells were then blocked for 1 h with PBS containing 10% FBS at 25°C before incubation with primary antibodies diluted in PBS containing 5% FBS at 4°C overnight. For immunofluorescence analysis of 5mC, following the treatment of 0.1% Triton X-100 in PBS, cells were exposed to 2N HCl for 20 min at 37°C to denature the double-strand DNA. After two rounds of neutralization with 0.1 M Borate, pH8.5 for 5 min at 25°C, cells were incubated with primary antibodies after a brief blocking step. Cells were washed three times with 0.1% Triton X-100 in PBS before incubating with Alexa Fluor 568 goat anti-mouse IgG1 (1:500) and Alexa Fluor 488 donkey anti-rabbit IgG (H + L) (1:500) in PBS for 1 h at 25°C under protection from light. After washing with 0.1% Triton X-100 in PBS, cells were mounted using SlowFade Antifade Mountant with DAPI. Images were acquired using Carl Zeiss LSM 710 and Carl Zeiss LSM 780 confocal microscopy at 40× magnification. Images were analyzed with ImageJ. The fluorescence of 5mC was quantified and normalized to DNA fluorescence from at least 100 cells positively stained for UHRF1 and DNMT1.

Identification of the acetylation sites by mass spectrometry

To identify the precise acetylation sites on UHRF1, we performed Mass Spectrometry analysis. 2 μg Purified UHRF1 and 2 μg MOF were incubated together for *in vitro* acetylation assay. The reaction mixtures were separated by SDS-PAGE, and the protein bands of UHRF1 were revealed by Coomassie Blue staining. Bands representing UHRF1 were excised from the gel, and two biological replicative samples were sent for Mass Spectrometry analysis served by BGI.

The proteolyzed peptides separated by liquid phase chromatography were ionized by a nanoESI source and then passed to a tandem mass spectrometer Q-Exactive HF X (Thermo Fisher Scientific, San Jose, CA) for DDA (Data Dependent Acquisition) mode detection. For the main parameters of the mass spectrometer, the ion source voltage was set to 1.9kV, the MS1 scanning range was 350~1,500m/z, the resolution was set to 60,000; MS2 starting m/z was fixed at 100, the resolution was 15,000. The ion screening conditions for MS2 fragmentation were charge 2+ to 6+, and the top 30 parent ions with the peak intensity exceeding 10,000. The ion fragmentation mode was HCD, and the fragment ions were detected in Orbitrap. The dynamic exclusion time was set to 30 s. The AGC was set to: MS1 3E6, MS2 1E5.

The identification of acetylated protein is mainly based on the experimental tandem mass spectrometry data, which is matched with the theoretical MS data from the database simulation so as to obtain the protein identification results. Raw MS data were searched against a human UHRF1 protein sequence (acquired from UniProt) using Maxquant (version 2.0.3.0). The following parameters were used for data processing: trypsin/P, with a maximum number of 4 missed cleavages; precursor and fragment ion mass tolerance was set to 10 ppm; variable modification was set to acetylation on lysine (K, 42.0106) and protein N terminus; fixed modification was set to Carbamidomethylation on cysteine (C, 57.0215); An algorithm of Percolator was used to keep peptide FDR less than 5%. Modification probability was kept at more than 0.75.

Cell-based ubiquitination assay

HEK293T cells were co-transfected with indicated plasmids. After treatment with 5 μM MG132 for 6 h, cells were lysed in Ubiquitination Lysis buffer (1% Nonidet P-40, 0.5% sodium deoxycholate, 0.1% SDS, 150 mM NaCl, 50 mM Tris·HCl, pH 8) containing 10 mM N-ethyl maleimide, protease inhibitors, and were sonicated for 30 s. Then cell lysates were centrifuged at 13,200 rpm for 10 min at 4°C and the supernatants were incubated with anti-FLAG M2 Agarose Beads (SIGMA) overnight at 4°C with gentle rotation. After 3 washes with Ubiquitination Wash buffer (1% Triton X-100, 50 mM HEPES pH 7.5, 150 mM NaCl, 5 mM EDTA, 0.05% SDS) containing 10 mM N-ethyl maleimide and protease inhibitor, protein samples were denatured in loading buffer by boiling, followed by SDS/PAGE and Western Blotting.

Bisulfite sequencing

Genomic DNA was extracted and purified with TIANamp Genomic DNA Kit (TIANGEN, DP304). For bisulfite conversion, one μg genomic DNA was treated and recovered using EpiTect Bisulfite kit (Qiagen 59104) following the manufacturer's manual. The IAP and LINE1 regions were amplified from bisulfite-converted genomic DNA via PCR using the following primer pairs: IAP F and IAP R, LINE1 F, and LINE1 R (Table S1). IAP and LINE1 amplicons were ligated into the pGEM-T vector (Promega) for cloning. Eight colonies were sequenced for each assay, and the sequencing data were analyzed by QUMA (http://quma.cdb.riken.jp/).

Reduced representation bisulfite sequencing (RRBS)

Total genomic DNA was extracted using TIANamp Genomic DNA Kit (TIANGEN, DP304). The double-enzyme RRBS library was prepared according to a previously published protocol.[52] The libraries were sequenced using Illumina NextSeq 500 system according to the manufacturer's instructions. For raw data filtration, low-quality bases were trimmed by using Trim Galore (version: 0.5.0). Adapter sequences (read1: -AGATCGGAAGAGCACACGTCTGAACTCCAGTCAC-; read2: - AGATCGGAAGAGCGTCGTGTAGGGAAAGAG TGTA-) were trimmed by using cutadapt implemented in Trim Galore. Low-quality bases were trimmed by using the following algorithm: Subtract 22 from all qualities; compute partial sums from all indices to the end of the sequence; cut sequence at the index at which the sum is minimal. Only reads whose length is not less than 30 after above process was retained. The parameters used were "trim_galore –stringency 4 –quality 22 –clip_R1 7 – clip_R2 7". The cleaned reads were mapped back to mouse genome (mm10) using BSMAP software version 2.73.[50] The parameters used were "bsmap -n 0 -v 0.08 -R -u -z 33". Methylation ratios were extracted from BSMAP output using a Python script (methratio.py), which is distributed with the BSMAP package. Only unique mapped reads were used to calculate methylation ratios. Only cytosines in a CpG context with sufficient sequencing depth (greater than or equal to 5x coverage) were retained for further analysis. Differentially methylated genes were determined by the software metilene[51] which identified and annotated differentially methylated regions. The parameters used were |difference of CpG methylation|≥0.1, number of differentially methylated CpG (DMC) ≥5, distance of neighboring DMC<=300bp, and q-value <0.05. All data analysis and visualization of CpG methylation and differentially methylated genes were conducted using R 4.3.1 (https://www.r-project.org/).

Double thymidine block

To synchronize cells in G1/S cell cycle phase, we performed a double thymidine block. The HEK 293T cells were passed onto 8 × 10cm dishes and grown to 20–30% confluency. Afterward, they were treated with 2mM thymidine for 18 h. Then they were washed with PBS twice and, changed to fresh medium and grown in 37°C, 5% CO_2 for 10 h, after which they were again treated with 2mM thymidine for 18 h. After the second block, they were released by washing with PBS twice and changing to fresh

medium, and then they were collected after 0, 1.5, 4.5, 6, 7.5, 9, 10.5, and 12 h after release so that the cells were collected at different cell cycle phase.

Subcellular fractionation

Cell pellets were resuspended in one cell volume of Hypotonic buffer (10 mM HEPES pH 7.5, 10 mM KCl, 1.5 mM $MgCl_2$, 0.5% Nonidet P-40). After incubation on ice for 10 min, cells were disrupted by 10 passages through a 25-gauge needle. Cells were centrifuged for 10 min at 1,000 × g at 4°C, and the supernatant containing the cytoplasmic fraction (S1) was collected by further centrifugation at 15,000 × g for 15 min. The remaining pellets were washed twice with Hypotonic buffer, resuspended in Hypertonic buffer (20 mM HEPES pH 7.5, 420 mM KCl, 1.5 mM $MgCl_2$, 0.5% Nonidet P-40), and incubated at 4°C for 30 min with gentle rotation. The supernatant containing the nuclear fraction (S2) was collected by centrifugation at 15,000 × g for 15 min. The remaining precipitates were chromatin-bound proteins (P2).

Electrophoretic mobility shift assay

Recombinant GST, GST–UHRF1, and GST-3KR-UHRF1 proteins were used in the experiment, and the 1 volume is around 0.5μg. To test their hemi-mCpG binding activity, 1,2 or 4 volumes of recombinant GST fused protein was incubated with 30bp hemi-mCpG DNA in the binding buffer (10 mM Tris-Cl (pH 7.5), 50 mM NaCl, 5 mM MgCl2, 1 mM DTT, 0.05% NP-40, 5% glycerol) at 4°C for 20 min. The reactions were then electrophoresed on a 6% polyacrylamide gel in 0.5x TBE buffer at 200 V for 0.5 h. The results were then visualized after incubation of the gel with EtBr (1:20000) for 15min. The sequences of the forward and reverse strands of the hemi-mCpG probes are upper strand 5′-TTGCACTCTCCTCCXGGAAGTCCCAGCTTC-3′ and lower strand 5′-GAAGCTGGGACTTCCGGGAG GAGAGTGCAA -3′, X = 5-methyldeoxycytosine.

QUANTIFICATION AND STATISTICAL ANALYSIS

The experiment results were analyzed with GraphPad Prism 6 software. All images or statistical results were based on at least three independent experiments. Analysis methods for mass spectrometry and RRBS data were shown in the previous **Identification of the acetylation sites by mass spectrometry** and **Reduced representation bisulfite sequencing (RRBS)** parts.